

On 2D Euler Equations: Part II. Lax Pairs and Homoclinic Structures

Yanguang (Charles) Li *

Department of Mathematics

University of Missouri

Columbia, MO 65211

e-mail: cli@math.missouri.edu

phone: 573-884-0622

fax: 573-882-1869

November 21, 2018

*This work is supported by the AMS Centennial Fellowship, and the Guggenheim Fellowship.

Abstract

In Part I [25] of our study on 2D Euler equation, we established the spectral theorem for a linearized 2D Euler equation. We also computed the point spectrum through continued fractions, and identified the eigenvalues with nonzero real parts.

In this Part II of our study, first we discuss the Lax pairs for both 2D and 3D Euler equations. The existence of Lax pairs suggests that the hyperbolic foliations of 2D and 3D Euler equations may be degenerate, i.e., there exist homoclinic structures. Then we investigate the question on the degeneracy v.s. nondegeneracy of the hyperbolic foliations for Galerkin truncations of 2D Euler equation. In particular, for a Galerkin truncation, we have computed the explicit representation of the hyperbolic foliation which is of the degenerate case, i.e., figure-eight case. We also study the robustness of this degeneracy for a so-called dashed-line model through higher order Melnikov functions. The first order and second order Melnikov functions are all identically zero, which indicates that the degeneracy is relatively robust. The study in this paper serves a clue in searching for homoclinic structures for 2D Euler equation. The recent breakthrough result [24] of mine on the existence of a Lax pair for 2D Euler equation, strongly supports the possible existence of homoclinic structures for 2D Euler equation.

PACS: 47.27 47.52 02.30.J 05.45 .

MSC: 76 34 35 37 .

Keywords: perverted heteroclinic orbit, higher order Melnikov function, degenerate hyperbolic foliation.

Contents

1	Introduction	4
2	Lax Pairs for 2D and 3D Euler Equations	6
2.1	The Lax Pair for 2D Euler Equation	6
2.2	The Lax Pair for 3D Euler Equation	8
3	Introduction of the Dashed-Line Model	9
3.1	Preliminaries on Linearized 2D Euler Equation	10
3.2	Rationality of the Dashed-Line Model	12
4	The Degenerate Hyperbolic Foliations of the Dashed-Line Model When $\epsilon = 0$	18
4.1	Invariant Subsystems When $\epsilon = 0$	18
4.2	Perverted Heteroclinic Orbits When $\epsilon = 0$	19
4.3	Discussion on the Perverted Heteroclinic Orbits	21
5	The Higher Order Melnikov Functions	23
5.1	The Melnikov Functions	23
5.2	The Derivation of Higher Order Melnikov Functions	24
5.3	Numerical Evaluations of the Second and Third Order Melnikov Functions	28
5.3.1	Numerical Evaluations of the Second Order Melnikov Functions . .	28
5.3.2	Numerical Evaluations of the Third Order Melnikov Functions . . .	31
6	Conclusion and Discussion	34

1 Introduction

In a series of works ([25], the current article, and [22]), we plan to build a dynamical system theory on 2D turbulence. The governing equation that we are interested in is the incompressible 2D Navier-Stokes equation under periodic boundary conditions. We are particularly interested in investigating the dynamics of 2D Navier-Stokes equation in the infinite Reynolds number limit and of 2D Euler equation. Our approach is different from many other studies on 2D Navier-Stokes equation in which one starts with Stokes equation to prove results on 2D Navier-Stokes equation for small Reynolds number. In our studies, we start with 2D Euler equation and view 2D Navier-Stokes equation for large Reynolds number as a (singular) perturbation of 2D Euler equation. 2D Euler equation is a Hamiltonian system with infinitely many Casimirs. To understand the nature of turbulence, we start with investigating the hyperbolic structure of 2D Euler equation. We are especially interested in investigating the degeneracy v.s. nondegeneracy nature of the hyperbolic foliation. Degeneracy means the coincidence of center-unstable and center-stable manifolds or unstable and stable foliations, i.e., figure-eight structure. If all the hyperbolic foliations of 2D Euler equation are of figure-eight, then there is no turbulent dynamics for 2D Euler equation.

The recent breakthrough result [24] of mine on the existence of a Lax pair for 2D Euler equation makes my idea in the last paragraph even more realistic. The philosophical significance of the existence of a Lax pair for 2D Euler equation by the author, and more recently for 3D Euler equation by Steve Childress [4], is beyond the particular project undertaken here. If one defines integrability of an equation by the existence of a Lax pair, then both 2D and 3D Euler equations are integrable. More importantly, both 2D and 3D Navier-Stokes equations at high Reynolds numbers are near integrable systems. Such a point of view changes our old ideology on Euler and Navier-Stokes equations.

In [25], we studied a linearized 2D Euler equation at a fixed point. The linear system decouples into infinitely many one-dimensional invariant subsystems. The essential spectrum of each invariant subsystem is a band of continuous spectrum on the imaginary axis. Only finitely many these invariant subsystems have point spectra. The point spectra can be computed through continued fractions. Examples show that there are indeed eigenvalues with positive and negative real parts. Thus, there is linear hyperbolicity. To understand the hyperbolic foliations of 2D Euler equation, especially the nature of degeneracy v.s. nondegeneracy of the hyperbolic foliations, we first study a Galerkin truncation. The Galerkin truncation presented in this article allows us to compute the hyperbolic foliation explicitly. We call this Galerkin truncation the *dashed-line model*. The dashed-line model contains a control parameter $\epsilon \in [0, 1]$. When the control parameter vanishes, the model decouples into a sequence of five-dimensional invariant subsystems. The eigenvalues of one of such invariant subsystems are “good” approximations of the eigenvalues of the original linearized 2D Euler equation. For this five-dimensional invariant subsystem, the hyperbolic foliation can be calculated explicitly with elegant formula representation. The hyperbolic foliation has the picture form of a “lip”. Both the upper and the lower halves of the “lip” are two-dimensional ellipsoidal surfaces. Orbits in each half of the “lip” are heteroclinic orbits spiraling into two fixed points as time approaches positive and negative infinities, and having a “turning point” (“perversion” [19] [13] [14] [15] [16] [18] [17]) in the

middle. We call these orbits *perverted heteroclinic orbits*. In terms of physical variables, such heteroclinic orbits represent heteroclinic profile-evolutions approaching two different stationary profiles as time approaches positive and negative infinities. Recently, there are more and more interests in studying heteroclinic and homoclinic orbits in fluids [8] [6] [7]. For the two-dimensional Kelvin-Helmholtz problem, Craig and Groves found a homoclinic orbit approaching a temporally periodic profile as time approaches positive and negative infinities for a fourth order normal form [7]. Numerical calculation indicates that the eigenvalues with zero real parts of the dashed-line model when the control parameter vanishes, form four narrow bands. When the control parameter is increased from 0 to 1, the sizes of these four bands increase and congregate into the one band continuous spectrum of the original linearized 2D Euler equation. In this sense, the eigenvalues with zero real parts of the dashed-line model approximate the continuous spectrum of the original linearized 2D Euler equation. We are interested in investigating the degeneracy v.s. nondegeneracy nature of the hyperbolic foliation for 2D Euler equation. As a first step, we will study the persistence of the “lip” structure for the dashed-line model through Melnikov functions. It turns out that both the first order and the second order Melnikov functions are identically zero.

There have been a lot of works on Melnikov functions since the original work of V. K. Melnikov [27]. It has been proved rigorously that a Melnikov function is the leading order term of a certain signed distance between center-unstable and center-stable manifolds, see for example [20] [33] [5] [26]. Typically, a Melnikov function is a temporal integral from negative infinity to positive infinity of the inner product of the gradient of certain invariant with the perturbation term evaluated along an unperturbed heteroclinic or homoclinic orbit, and this integrand often has exponential decay property as time approaches positive and negative infinities. The importance of Melnikov functions is to determine the intersection between the center-unstable and the center-stable manifolds. The argument is as follows. Often the Melnikov function is easily computable. First one seeks zeros for the Melnikov functions; then implicit function theorem implies nearby zeros for the signed distance. The intersection between the center-unstable and the center-stable manifolds implies the existence of orbits homoclinic to the center manifold. Other variety of Melnikov functions include subharmonic Melnikov functions [20], which are temporal integrals over the finite period intervals, and exponentially small Melnikov functions [12], etc. In some special circumstance, the Melnikov function can be identically zero as a function of parameters. In such case, one needs to calculate the next leading order term of the signed distance, called the *second order Melnikov function*. If the $(n - 1)$ -th order Melnikov function is identically zero as a function of the parameters, the n -th order *Melnikov function* serves as the leading order term of the signed distance. There have been some works on second order Melnikov functions, see for example [29] [30] [34] [28] [9] [21]. In this paper, we are going to derive high order Melnikov functions without rigorous justification for the dashed-line model, and calculate them to study the persistence of the figure-eight structure.

Our purpose of introducing the dashed-line model is for investigating the hyperbolic foliation of 2D Euler equation, which is different from those of other models. For example, the shell model [3] [32] models the interaction of energy in different shells in the spectral space. The difference between the dashed-line model and the shell model can be summarized as follows: 1. The nonlinear terms in the dashed-line model are derived from Galerkin

truncations, while the nonlinear terms in the shell model are postulated. On the other hand, both the dashed-line model and the shell model conserve the energy and the enstrophy. 2. The dashed-line model captures the eigenvalues of the linearized 2D Euler equation, while the shell model has no such information at all. 3. The dashed-line model is claimed to model the dynamics of the 2D Euler equation in a neighborhood of a line of fixed points and hopefully also the global dynamics. The variables in the dashed-line model have precise physical meanings. The shell model is claimed to model the transfer of energy in different spectral shells. The variables in the shell model are artificial.

The article is organized as follows: In Section 2, we discuss the Lax pairs for both 2D and 3D Euler equations. In Section 3, we will introduce the dashed-line model and discuss its rationality. In Section 4, we will compute explicitly the figure-eight structure for the dashed-line model at the special parameter value $\epsilon = 0$. In Section 5, we study the persistence of the figure-eight structure when $\epsilon \neq 0$ through higher order Melnikov functions. Section 6 is the conclusion.

2 Lax Pairs for 2D and 3D Euler Equations

In this section, we are going to discuss the most recent results on the Lax pairs of 2D and 3D Euler equations.

2.1 The Lax Pair for 2D Euler Equation

We consider the two-dimensional incompressible Euler equation written in vorticity form,

$$\frac{\partial \Omega}{\partial t} = -u \frac{\partial \Omega}{\partial x} - v \frac{\partial \Omega}{\partial y} , \tag{2.1}$$

$$\frac{\partial u}{\partial x} + \frac{\partial v}{\partial y} = 0 ;$$

where Ω is vorticity, u and v are respectively velocity components along x and y directions. If we define the stream function Ψ by,

$$u = -\frac{\partial \Psi}{\partial y} , \quad v = \frac{\partial \Psi}{\partial x} ,$$

then we have the relation between vorticity Ω and stream function Ψ ,

$$\Omega = \frac{\partial v}{\partial x} - \frac{\partial u}{\partial y} = \Delta \Psi .$$

The 2D Euler equation (2.1) can be written in the equivalent form,

$$\frac{\partial \Omega}{\partial t} + \{\Psi, \Omega\} = 0 , \tag{2.2}$$

where the bracket $\{ \}$ is defined as

$$\{f, g\} = (\partial_x f)(\partial_y g) - (\partial_y f)(\partial_x g) .$$

Theorem 2.1 ([24]) *The Lax pair of the 2D Euler equation (2.2) is given as*

$$\begin{cases} L\varphi = \lambda\varphi , \\ \partial_t\varphi + A\varphi = 0 , \end{cases} \quad (2.3)$$

where

$$L\varphi = \{\Omega, \varphi\} , \quad A\varphi = \{\Psi, \varphi\} ,$$

and λ is a complex constant, and φ is a complex-valued function.

The compatibility condition of the Lax pair (2.3) gives the 2D Euler equation (2.2), i.e.

$$\partial_t L = [L, A] ,$$

where $[L, A] = LA - AL$, gives the Lax representation of the 2D Euler equation (2.2). In investigating 2D Euler equation through the Lax pair, two areas seem promising. The first area is Darboux transformation. Darboux transformations have been utilized for generating explicit representations for homoclinic structures for soliton equations, see for example [23]. Up to now, the Darboux transformation for the above Lax pair has not been found. On the other hand, in the present paper, we do not use the approach of Darboux transformation for investigating homoclinic structures for 2D Euler equation, rather use the classical approach of Galerkin truncations. Investigating the Darboux transformation is our future research. The other area is inverse scattering transform. Inverse scattering transforms have been exploited for solving the Cauchy problems of soliton equations, see for example [11] [2]. In building the inverse scattering, it is crucial to have constant coefficient differential operators in (especially the spatial part of) the Lax pair. For that reason, one may start with the following Lax pair [35],

$$\begin{cases} D_1\varphi + \{\Omega, \varphi\} = \lambda\varphi , \\ \partial_t\varphi + D_2\varphi + \{S, \varphi\} = 0 , \end{cases} \quad (2.4)$$

where

$$D_1 = \alpha \frac{\partial}{\partial x} + \beta \frac{\partial}{\partial y} , \quad D_2 = \gamma \frac{\partial}{\partial x} + \delta \frac{\partial}{\partial y} ,$$

α, β, γ , and δ are real constants, λ is a complex constant, S is a real-valued function, and φ is a complex-valued function. The compatibility condition of this Lax pair gives the following equation instead of the 2D Euler equation,

$$\frac{\partial\Omega}{\partial t} + \{S, \Omega\} + D_2\Omega - D_1S = 0. \quad (2.5)$$

A promising approach is that one can first build the inverse scattering for (2.4) and (2.5), and then take the limits

$$\alpha, \beta, \gamma, \delta \rightarrow 0 , \quad S \rightarrow \Psi = \Delta^{-1}\Omega ,$$

to get results for 2D Euler equation. A special case of the Equation (2.5) is the following system of equations [35],

$$\begin{cases} \frac{\partial \Omega}{\partial t} + \{S, \Omega\} = 0 , \\ D_1 S = D_2 \Omega . \end{cases}$$

In this paper, we are not going to follow the approach of inverse scattering transform either. Investigating the inverse scattering transform is our future research. Here the Lax pair structures make it plausible for the existence of homoclinic structures for the 2D Euler equation.

2.2 The Lax Pair for 3D Euler Equation

We consider the three-dimensional incompressible Euler equation written in vorticity form,

$$\partial_t \Omega + (u \cdot \nabla) \Omega - (\Omega \cdot \nabla) u = 0 , \quad (2.6)$$

where $u = (u_1, u_2, u_3)$ is the velocity, $\Omega = (\Omega_1, \Omega_2, \Omega_3)$ is the vorticity, $\Omega = \nabla \times u$, and $\nabla \cdot u = 0$. u can be represented by Ω for example through Biot-Savart law. More recently, to the author's surprise, the Lax pair for 3D Euler equation was established by Steve Childress.

Theorem 2.2 ([4]) *The Lax pair of the 3D Euler equation (2.6) is given as*

$$\begin{cases} L\varphi = \lambda\varphi , \\ \partial_t \varphi + A\varphi = 0 , \end{cases} \quad (2.7)$$

where

$$L\varphi = \Omega \cdot \nabla \varphi - \varphi \cdot \nabla \Omega , \quad A\varphi = u \cdot \nabla \varphi - \varphi \cdot \nabla u ,$$

λ is a complex constant, and $\varphi = (\varphi_1, \varphi_2, \varphi_3)$ is a complex 3-vector valued function.

The compatibility condition of the Lax pair (2.7) gives the 3D Euler equation (2.6), i.e.

$$\partial_t L = [L, A] ,$$

where $[L, A] = LA - AL$, gives the Lax representation of the 3D Euler equation (2.6).

Unfortunately, when one does 2D reduction to the Lax pair (2.7), one gets $L = 0$. Therefore, the Lax pair (2.7) does not imply any Lax pair for 2D Euler equation.

In investigating 3D Euler equation through the Lax pair, especially the question on the possibility of finite time blow up solutions, the two areas: (1). Darboux transformations, (2). inverse scattering transforms, also seem promising. Up to now, the Darboux transformation for the Lax pair (2.7) has not been found. Investigating the Darboux transformation and the inverse scattering transform for the Lax pair (2.7) is our future research.

In building the inverse scattering, it is crucial to have constant coefficient differential operators in (especially the spatial part of) the Lax pair. For 3D Euler equation, we may start with the following Lax pair

Proposition 1 *We consider the following Lax pair,*

$$\begin{cases} L\varphi = \lambda\varphi , \\ \partial_t\varphi + A\varphi = 0 , \end{cases} \quad (2.8)$$

where

$$L\varphi = \Omega \cdot \nabla\varphi - \varphi \cdot \nabla\Omega + D_1\varphi , \quad A\varphi = q \cdot \nabla\varphi - \varphi \cdot \nabla q + D_2\varphi ,$$

λ is a complex constant, $\varphi = (\varphi_1, \varphi_2, \varphi_3)$ is a complex 3-vector valued function, $q = (q_1, q_2, q_3)$ is a real 3-vector valued function, $D_j = \alpha^{(j)} \cdot \nabla$, ($j = 1, 2$), $\alpha^{(j)} = (\alpha_1^{(j)}, \alpha_2^{(j)}, \alpha_3^{(j)})$ are real constant 3-vectors. The compatibility condition of this Lax pair gives the following equation instead of the 3D Euler equation,

$$\partial_t\Omega + (q \cdot \nabla)\Omega - (\Omega \cdot \nabla)q + D_2\Omega - D_1q = 0 . \quad (2.9)$$

A specialization of (2.9) is the following system of equations,

$$\begin{cases} \partial_t\Omega + (q \cdot \nabla)\Omega - (\Omega \cdot \nabla)q = 0 , \\ D_1q = D_2\Omega . \end{cases}$$

Proof: The proof of this proposition is a trivial direct verification. \square

A promising approach is that one can first build the inverse scattering for (2.8), and then take the limits

$$\alpha^{(j)} \rightarrow 0 , \quad (j = 1, 2) , \quad q \rightarrow u ,$$

to get results for 3D Euler equation. Here the Lax pair structures make it plausible for the existence of homoclinic structures for the 3D Euler equation based upon the study on soliton equations [23].

Remark 2.1 *If one defines integrability of an equation by the existence of a Lax pair, then both 2D and 3D Euler equations are integrable. More importantly, both 2D and 3D Navier-Stokes equations at high Reynolds numbers are near integrable systems.*

3 Introduction of the Dashed-Line Model

We consider the two-dimensional incompressible Euler equation written in vorticity form(2.1) under periodic boundary conditions in both x and y directions with period 2π . We also require that both u and v have means zero,

$$\int_0^{2\pi} \int_0^{2\pi} u \, dx dy = \int_0^{2\pi} \int_0^{2\pi} v \, dx dy = 0.$$

We expand Ω into Fourier series,

$$\Omega = \sum_{k \in \mathbb{Z}^2 / \{0\}} \omega_k e^{ik \cdot X} ,$$

where $\omega_{-k} = \overline{\omega_k}$, $k = (k_1, k_2)^T$, $X = (x, y)^T$. In this paper, we confuse 0 with $(0, 0)^T$, the context will always make it clear. By the relation between vorticity Ω and stream function Ψ , the system (2.1) can be rewritten as the following kinetic system,

$$\dot{\omega}_k = \sum_{k=p+q} A(p, q) \omega_p \omega_q, \quad (3.1)$$

where $A(p, q)$ is given by,

$$\begin{aligned} A(p, q) &= \frac{1}{2} [|q|^{-2} - |p|^{-2}] (p_1 q_2 - p_2 q_1) \\ &= \frac{1}{2} [|q|^{-2} - |p|^{-2}] \begin{vmatrix} p_1 & q_1 \\ p_2 & q_2 \end{vmatrix}, \end{aligned} \quad (3.2)$$

where $|q|^2 = q_1^2 + q_2^2$ for $q = (q_1, q_2)^T$, similarly for p .

For any two functionals F_1 and F_2 of $\{\omega_k\}$, we define their Lie-Poisson bracket as

$$\{F_1, F_2\} = \sum_{k+p+q=0} \begin{vmatrix} q_1 & p_1 \\ q_2 & p_2 \end{vmatrix} \omega_k \frac{\partial F_1}{\partial \overline{\omega_p}} \frac{\partial F_2}{\partial \overline{\omega_q}}. \quad (3.3)$$

Then the 2D Euler equation (3.1) is a Hamiltonian system [1],

$$\dot{\omega}_k = \{\omega_k, H\}, \quad (3.4)$$

where the Hamiltonian H is the kinetic energy,

$$H = \frac{1}{2} \sum_{k \in \mathbb{Z}^2 / \{0\}} |k|^{-2} |\omega_k|^2. \quad (3.5)$$

Following are Casimirs (i.e. invariants that Poisson commute with any functional) of the Hamiltonian system (3.4):

$$J_n = \sum_{k_1 + \dots + k_n = 0} \omega_{k_1} \cdots \omega_{k_n}. \quad (3.6)$$

3.1 Preliminaries on Linearized 2D Euler Equation

In this subsection, we discuss the preliminary results on linearized 2D Euler equation known from [25].

We denote $\{\omega_k\}_{k \in \mathbb{Z}^2 / \{0\}}$ by ω . We consider the simple fixed point ω^* :

$$\omega_p^* = \Gamma, \quad \omega_k^* = 0, \quad \text{if } k \neq p \text{ or } -p, \quad (3.7)$$

of the 2D Euler equation (3.1), where Γ is an arbitrary complex constant. The *linearized two-dimensional Euler equation* at ω^* is given by,

$$\dot{\omega}_k = A(p, k-p) \Gamma \omega_{k-p} + A(-p, k+p) \bar{\Gamma} \omega_{k+p} . \quad (3.8)$$

Definition 1 (Classes) For any $\hat{k} \in Z^2/\{0\}$, we define the class $\Sigma_{\hat{k}}$ to be the subset of $Z^2/\{0\}$:

$$\Sigma_{\hat{k}} = \left\{ \hat{k} + np \in Z^2/\{0\} \mid n \in Z, \ p \text{ is specified in (3.7)} \right\}.$$

See Fig.3.1 for an illustration of the classes. According to the classification defined in Definition 1, the linearized two-dimensional Euler equation (3.8) decouples into infinitely many *invariant subsystems*:

$$\begin{aligned} \dot{\omega}_{\hat{k}+np} &= A(p, \hat{k} + (n-1)p) \Gamma \omega_{\hat{k}+(n-1)p} \\ &+ A(-p, \hat{k} + (n+1)p) \bar{\Gamma} \omega_{\hat{k}+(n+1)p} . \end{aligned} \quad (3.9)$$

Theorem 3.1 The eigenvalues of the linear operator $\mathcal{L}_{\hat{k}}$ defined by the right hand side of (3.9), are of four types: real pairs $(c, -c)$, purely imaginary pairs $(id, -id)$, quadruples $(\pm c \pm id)$, and zero eigenvalues.

The eigenvalues can be computed through continued fractions.

Definition 2 (The Disk) The disk of radius $|p|$ in $Z^2/\{0\}$, denoted by $D_{|p|}$, is defined as

$$D_{|p|} = \left\{ k \in Z^2/\{0\} \mid |k| < |p| \right\}.$$

The closure of $D_{|p|}$, denoted by $\bar{D}_{|p|}$, is defined as

$$\bar{D}_{|p|} = \left\{ k \in Z^2/\{0\} \mid |k| \leq |p| \right\}.$$

See Fig.3.1 for an illustration.

Theorem 3.2 (The Spectral Theorem) We have the following claims on the spectra of the linear operator $\mathcal{L}_{\hat{k}}$:

1. If $\Sigma_{\hat{k}} \cap \bar{D}_{|p|} = \emptyset$, then the entire ℓ_2 spectrum of the linear operator $\mathcal{L}_{\hat{k}}$ is its continuous spectrum. See Figure 3.2, where $b = -\frac{1}{2}|\Gamma||p|^{-2} \begin{vmatrix} p_1 & \hat{k}_1 \\ p_2 & \hat{k}_2 \end{vmatrix}$.
2. If $\Sigma_{\hat{k}} \cap \bar{D}_{|p|} \neq \emptyset$, then the entire essential ℓ_2 spectrum of the linear operator $\mathcal{L}_{\hat{k}}$ is its continuous spectrum. That is, the residual spectrum of $\mathcal{L}_{\hat{k}}$ is empty, $\sigma_r(\mathcal{L}_{\hat{k}}) = \emptyset$. The point spectrum of $\mathcal{L}_{\hat{k}}$ is symmetric with respect to both real and imaginary axes. See Figure 3.3.

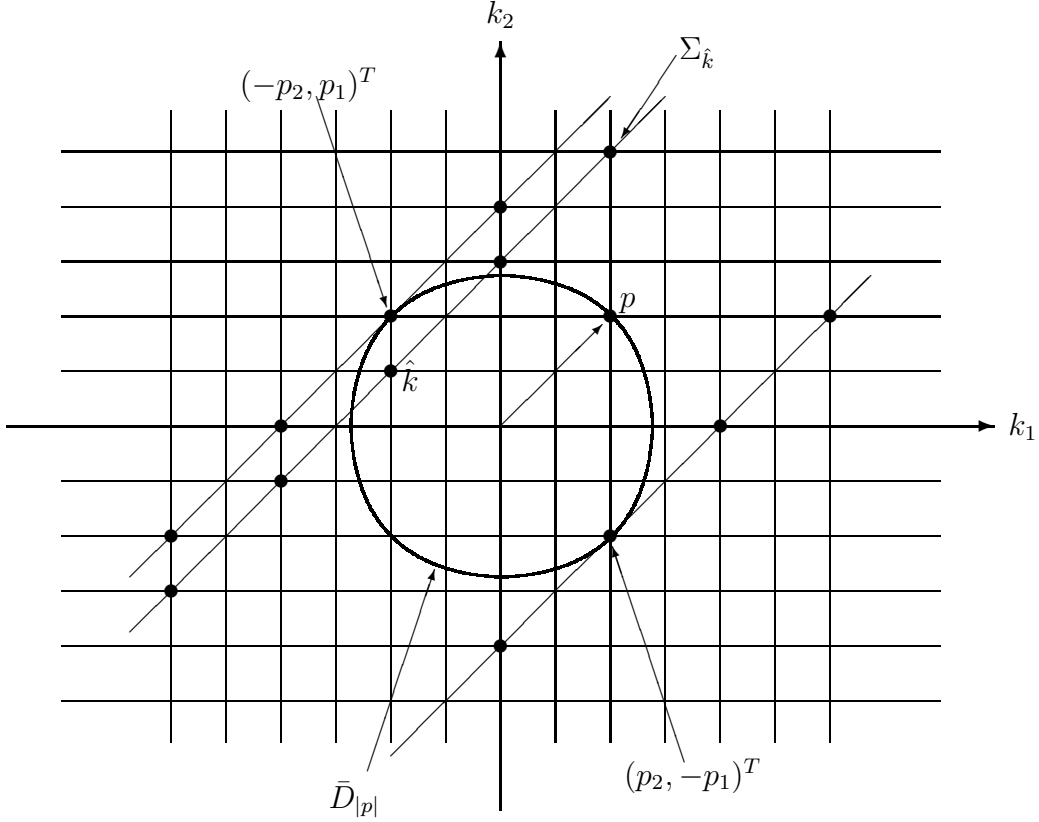


Figure 3.1: An illustration of the classes $\Sigma_{\hat{k}}$ and the disk $\bar{D}_{|p|}$.

3.2 Rationality of the Dashed-Line Model

To simplify our study, we study only the case when ω_k is real, $\forall k \in Z^2/\{0\}$, i.e. we only study the cosine transform of the vorticity,

$$\Omega = \sum_{k \in Z^2/\{0\}} \omega_k \cos(k \cdot X) ,$$

and the 2D Euler equation (2.1;3.1) preserves the cosine transform. To further simplify our study, we will study a concrete dashed-line model based upon the line of fixed points (3.7) with the mode $p = (1, 1)^T$ parametrized by Γ . When $\Gamma \neq 0$, each fixed point has 4 eigenvalues which form a quadruple. These four eigenvalues appear in the only unstable invariant linear subsystem labeled by $\hat{k} = (-3, -2)^T$. We computed the eigenvalues through continued fractions, one of them is [25]:

$$\tilde{\lambda} = 2\lambda/|\Gamma| = 0.24822302478255 + i 0.35172076526520 . \quad (3.10)$$

See Figure 3.4 for an illustration. We hope that a Galerkin truncation with a small number of modes including those inside the disk $\bar{D}_{|p|}$ can capture the eigenvalues. We propose the Galerkin truncation to the linear system (3.9) with the four modes $\hat{k} + p$, $\hat{k} + 2p$, $\hat{k} + 3p$, and $\hat{k} + 4p$,

$$\dot{\omega}_1 = -A_2\Gamma\omega_2 ,$$

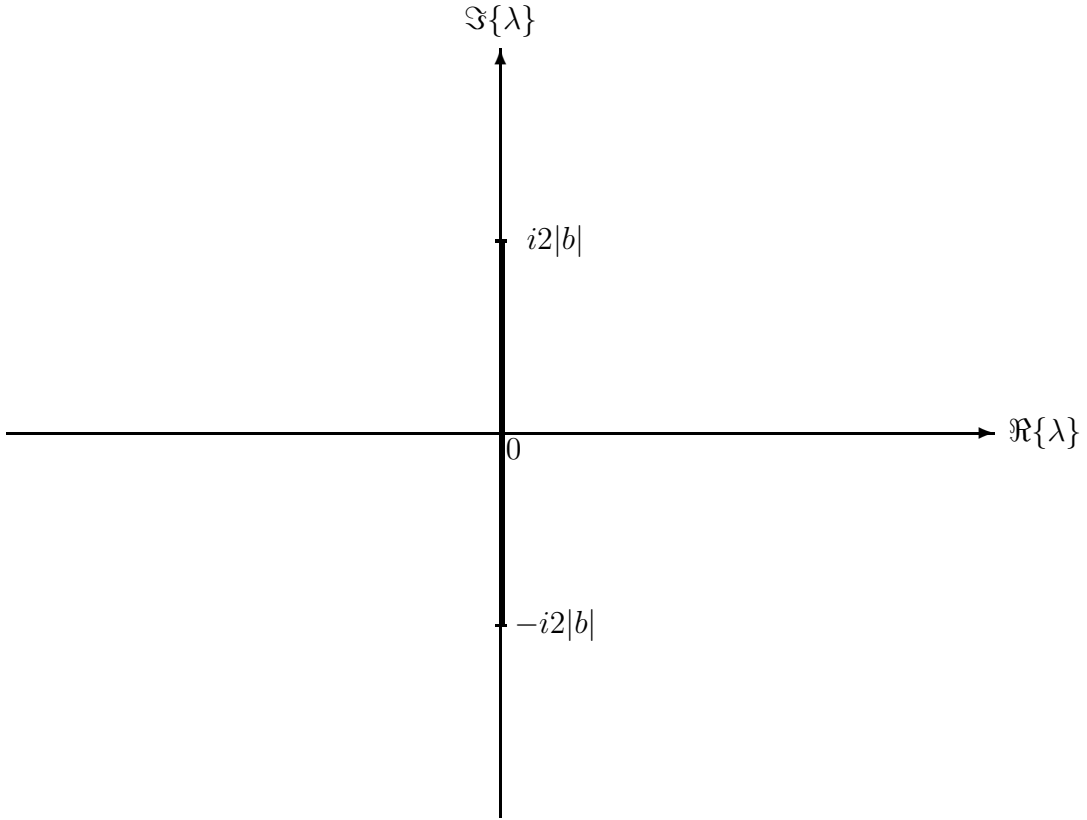


Figure 3.2: The spectrum of $\mathcal{L}_{\hat{k}}$ in case 1.

$$\begin{aligned}\dot{\omega}_2 &= A_1\Gamma\omega_1 - A_3\Gamma\omega_3, \\ \dot{\omega}_3 &= A_2\Gamma\omega_2 - A_4\Gamma\omega_4, \\ \dot{\omega}_4 &= A_3\Gamma\omega_3.\end{aligned}$$

From now on, the abbreviated notations,

$$\omega_n = \omega_{\hat{k}+np}, \quad A_n = A(p, \hat{k} + np), \quad A_{m,n} = A(\hat{k} + mp, \hat{k} + np), \quad (3.11)$$

will be used. The eigenvalues of this four dimensional system can be easily calculated. It turns out that this system has a quadruple of eigenvalues:

$$\begin{aligned}\lambda &= \pm \frac{\Gamma}{2\sqrt{10}} \sqrt{1 \pm i\sqrt{35}} \\ &\doteq \pm \left(\frac{\Gamma}{2}\right) \times 0.7746 \times e^{\pm i\theta_1},\end{aligned} \quad (3.12)$$

where $\theta_1 = \arctan(0.845)$, in comparison with the quadruple of eigenvalues (3.10), where

$$\lambda \doteq \pm \left(\frac{\Gamma}{2}\right) \times 0.43 \times e^{\pm i\theta_2},$$

and $\theta_2 = \arctan(1.418)$. Thus, *the quadruple of eigenvalues of the original system is recovered by the four-mode truncation.* Along the above line of thinking, we “chop” the line

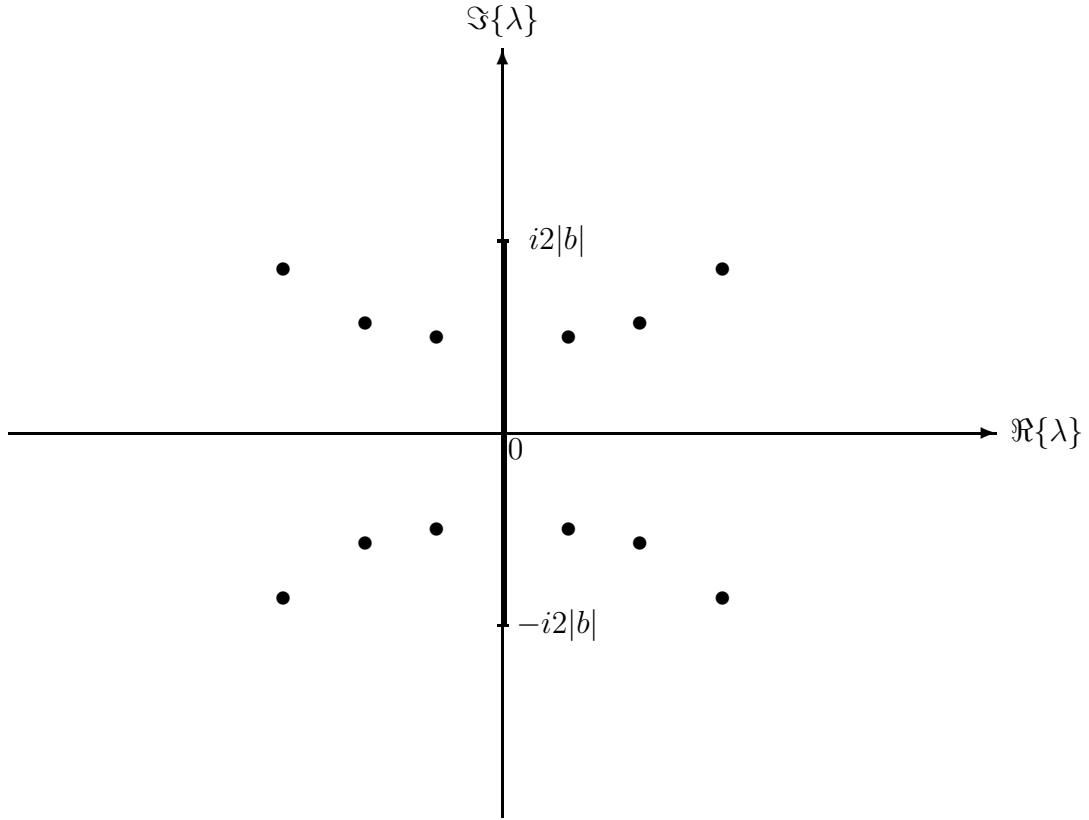


Figure 3.3: The spectrum of $\mathcal{L}_{\hat{k}}$ in case 2.

$\Sigma_{\hat{k}}$ as follows,

$$\begin{aligned}
 \dot{\omega}_{5j+1} &= -A_{5j+2} \Gamma \omega_{5j+2}, \\
 \dot{\omega}_{5j+2} &= A_{5j+1} \Gamma \omega_{5j+1} - A_{5j+3} \Gamma \omega_{5j+3}, \\
 \dot{\omega}_{5j+3} &= A_{5j+2} \Gamma \omega_{5j+2} - A_{5j+4} \Gamma \omega_{5j+4}, \\
 \dot{\omega}_{5j+4} &= A_{5j+3} \Gamma \omega_{5j+3}.
 \end{aligned}$$

That is, we “chop” the line $\Sigma_{\hat{k}}$ at the points $n = 5j$, $\forall j \in Z$. When $j \neq 0$, this system has two complex conjugate pairs of purely imaginary eigenvalues,

$$\lambda = \pm i(\Gamma/\sqrt{2})\sqrt{|b + \delta \sqrt{b^2 - 4c}|}, \quad \delta = \pm;$$

where

$$\begin{aligned}
 b &= -A_{5j+1}A_{5j+2} - A_{5j+2}A_{5j+3} - A_{5j+3}A_{5j+4}, \\
 c &= A_{5j+1}A_{5j+2}A_{5j+3}A_{5j+4}, \\
 b &< 0, \quad c > 0, \quad 0 < b^2 - 4c < b^2.
 \end{aligned}$$

When $j \rightarrow \pm\infty$,

$$\lambda \rightarrow \pm i(\Gamma/2)\sqrt{\frac{3 + \delta \sqrt{5}}{2}}, \quad \delta = \pm,$$

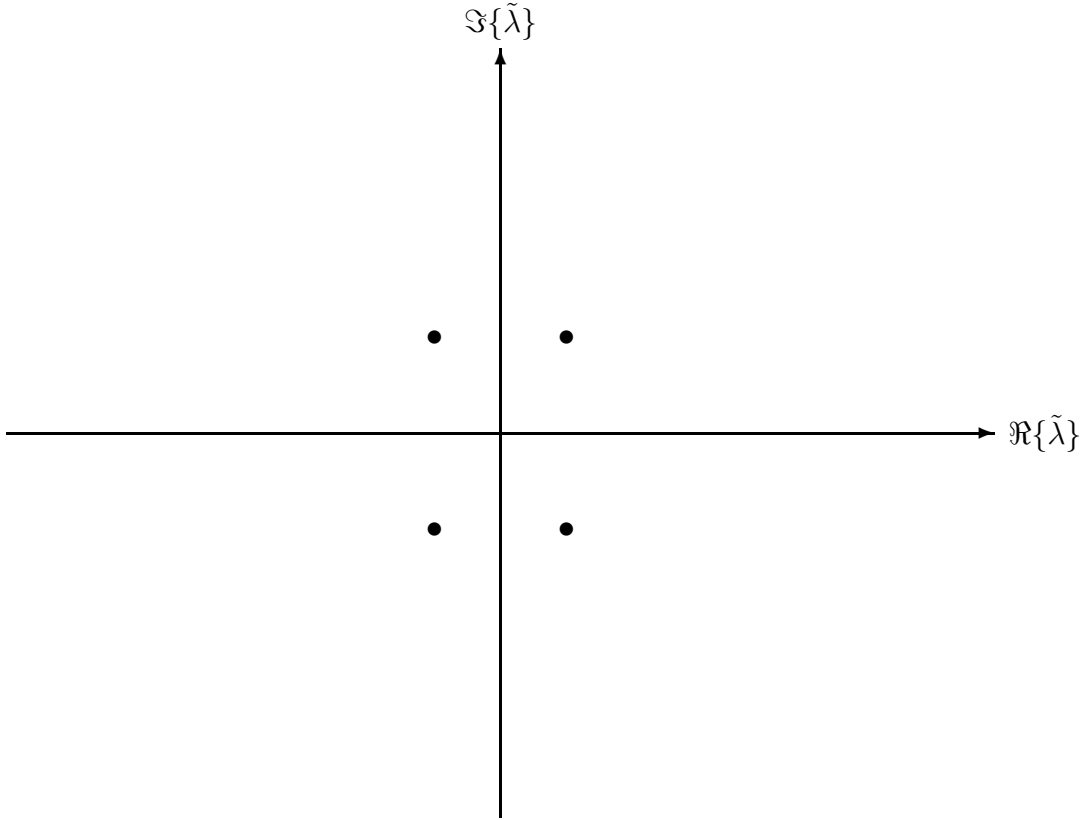


Figure 3.4: The quadruple of eigenvalues of the invariant system labeled by $\hat{k} = (-3, -2)^T$, when $p = (1, 1)^T$.

$$\doteq \pm i 0.31 \Gamma, \quad \pm i 0.8 \Gamma .$$

For example, when $j = 1$,

$$\lambda \doteq \pm i 0.2937609 \Gamma, \quad \pm i 0.7736967 \Gamma ;$$

when $j = 2$,

$$\lambda \doteq \pm i 0.3057701 \Gamma, \quad \pm i 0.8007493 \Gamma .$$

For all $j \in Z$, the distribution of the eigenvalues is illustrated in Fig.3.5. To recover the original linear system from the “chopped” system, we introduce the homotopy parameter $\epsilon \in [0, 1]$, and consider the homotopy system,

$$\dot{\omega}_n = \epsilon_{n-1} A_{n-1} \Gamma \omega_{n-1} - \epsilon_{n+1} A_{n+1} \Gamma \omega_{n+1}$$

where

$$\epsilon_n = \begin{cases} 1, & \text{if } n \neq 5j, \forall j \in Z, \\ \epsilon, & \text{if } n = 5j, \text{ for some } j \in Z. \end{cases}$$

The homotopy deformation of the spectra for this homotopy system is calculated numerically by Thomas Witelski and shown in Fig. 3.6 for a special value of Γ . As ϵ is increased from 0 to 1, the quadruple of eigenvalues moves along a curve, and the sizes of the four

Figure 3.5: The distribution of the eigenvalues of the chopped system.

Figure 3.6: The homotopy deformation of the spectra for the homotopy system.

bands of eigenvalues with zero real parts increase, and finally these four bands congregate into one band when $\epsilon = 1$ which is the continuum spectrum. From such numerical calculation, one can clearly see the homotopy transition of the spectra from a decoupled “chopped” subsystem to the original linearized 2D Euler equation. From the above discussions, it is natural to propose the following *dashed-line model*,

$$\begin{aligned}\dot{\omega}_n &= \epsilon_{n-1}A_{n-1}\omega_p\omega_{n-1} - \epsilon_{n+1}A_{n+1}\omega_p\omega_{n+1}, \\ \dot{\omega}_p &= -\sum_{n \in \mathbb{Z}} \epsilon_n \epsilon_{n-1} A_{n-1,n} \omega_{n-1} \omega_n,\end{aligned}\tag{3.13}$$

to model the hyperbolic structure of the 2D Euler equation, connected to the line of fixed points (3.7) with $p = (1, 1)^T$. Figure 3.7 illustrates the collocation of the modes in this model, which has the “*dashed-line*” nature leading to the name of the model.

The dashed-line model has the same properties as 2D Euler equation, of conserving the kinetic energy and enstrophy, and being a Hamiltonian system with the same Lie-Poisson bracket structure. For any two functionals F_1 and F_2 , we define their Lie-Poisson bracket as follows,

$$\{F_1, F_2\} = \sum_{k+q+r=0} \begin{vmatrix} r_1 & q_1 \\ r_2 & q_2 \end{vmatrix} \epsilon_k \omega_k \frac{\partial F_1}{\partial \omega_{-q}} \frac{\partial F_2}{\partial \omega_{-r}}.$$

The kinetic energy is given by,

$$\tilde{H} = \frac{1}{2} \left\{ \sum_{n \in \mathbb{Z}} \epsilon_n |\hat{k} + np|^{-2} \omega_{\hat{k}+np} \omega_{-\hat{k}+np} + |p|^{-2} \omega_p \omega_{-p} \right\}.$$

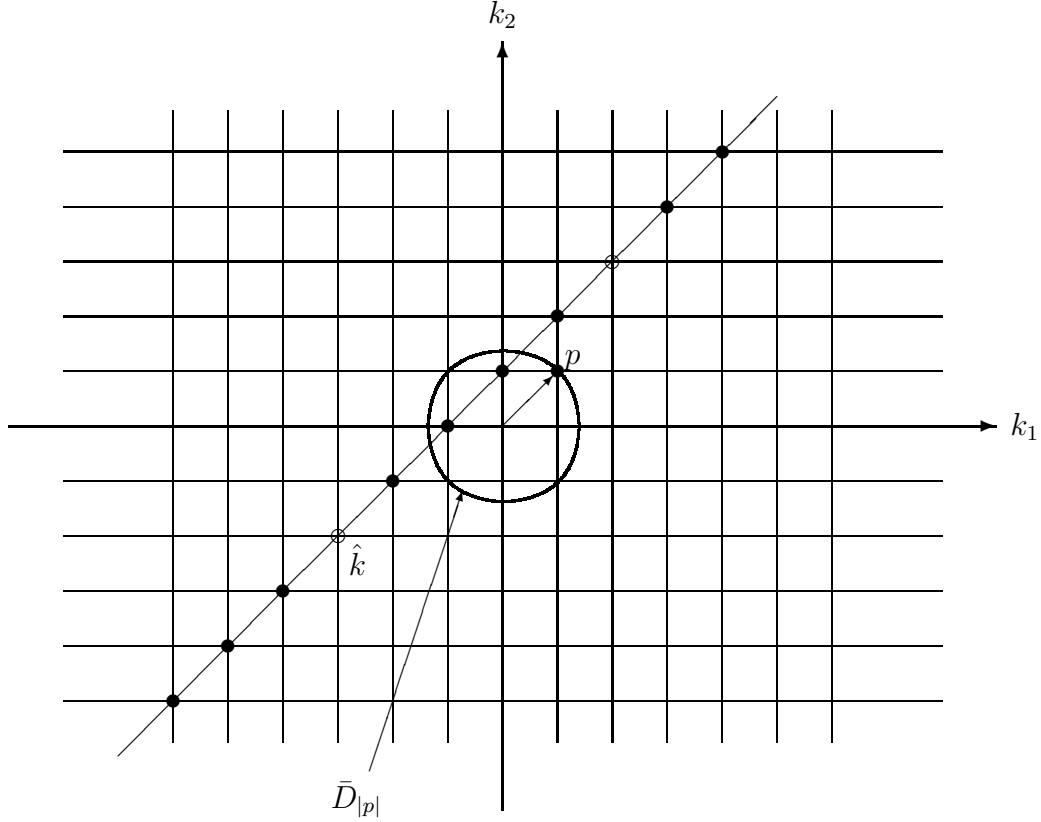


Figure 3.7: The collocation of the modes in the dashed-line model.

The dashed-line model (3.13) is a Hamiltonian system with the kinetic energy as the Hamiltonian,

$$\begin{cases} \dot{\omega}_{\hat{k}+np} = \{\omega_{\hat{k}+np}, \tilde{H}\} , \\ \dot{\omega}_p = \{\omega_p, \tilde{H}\} . \end{cases}$$

The enstrophy

$$\tilde{J}_2 = \omega_p \omega_{-p} + \sum_{n \in \mathbb{Z}} \epsilon_n \omega_{\hat{k}+np} \omega_{-[\hat{k}+np]}$$

is still a constant of motion. The invariance of kinetic energy and enstrophy is a consequence of the simple relations,

$$\begin{cases} \frac{1}{|k|^2} A(p, q) + \frac{1}{|p|^2} A(q, k) + \frac{1}{|q|^2} A(k, p) = 0 , \\ A(p, q) + A(q, k) + A(k, p) = 0 ; \end{cases}$$

whenever $k + p + q = 0$.

The dashed-line model is also a homotopy system parametrized by the homotopy parameter $\epsilon \in [0, 1]$. When $\epsilon = 0$, the figure-eight hyperbolic structure of the dashed-line model is computable as studied in next section. As a first step toward understanding the homotopy deformation of such hyperbolic structure, we are going to use higher order Melnikov functions to study the persistence of such figure-eight hyperbolic structure when ϵ is small.

4 The Degenerate Hyperbolic Foliations of the Dashed-Line Model When $\epsilon = 0$

When $\epsilon = 0$, the dashed-line model takes the form:

$$\begin{aligned}
\dot{\omega}_{5j+1} &= -A_{5j+2}\omega_p\omega_{5j+2}, \\
\dot{\omega}_{5j+2} &= A_{5j+1}\omega_p\omega_{5j+1} - A_{5j+3}\omega_p\omega_{5j+3}, \\
\dot{\omega}_{5j+3} &= A_{5j+2}\omega_p\omega_{5j+2} - A_{5j+4}\omega_p\omega_{5j+4}, \quad (j \in Z), \\
\dot{\omega}_{5j+4} &= A_{5j+3}\omega_p\omega_{5j+3}, \\
\dot{\omega}_p &= -\sum_{j \in Z} \left[A_{5j+1,5j+2}\omega_{5j+1}\omega_{5j+2} + A_{5j+2,5j+3}\omega_{5j+2}\omega_{5j+3} \right. \\
&\quad \left. + A_{5j+3,5j+4}\omega_{5j+3}\omega_{5j+4} \right],
\end{aligned} \tag{4.1}$$

and the equation for the decoupled variable ω_{5j} is given by,

$$\dot{\omega}_{5j} = A_{5j-1}\omega_p\omega_{5j-1} - A_{5j+1}\omega_p\omega_{5j+1}.$$

This system has a sequence of invariant subsystems, one of which carries the hyperbolic structure.

4.1 Invariant Subsystems When $\epsilon = 0$

For each fixed $j \in Z$, we have the seven dimensional invariant subsystems:

$$\begin{aligned}
\dot{\omega}_{5j+1} &= -A_{5j+2}\omega_p\omega_{5j+2}, \\
\dot{\omega}_{5j+2} &= A_{5j+1}\omega_p\omega_{5j+1} - A_{5j+3}\omega_p\omega_{5j+3}, \\
\dot{\omega}_{5j+3} &= A_{5j+2}\omega_p\omega_{5j+2} - A_{5j+4}\omega_p\omega_{5j+4}, \\
\dot{\omega}_{5j+4} &= A_{5j+3}\omega_p\omega_{5j+3}, \\
\dot{\omega}_p &= -[A_{5j+1,5j+2}\omega_{5j+1}\omega_{5j+2} + A_{5j+2,5j+3}\omega_{5j+2}\omega_{5j+3} \\
&\quad + A_{5j+3,5j+4}\omega_{5j+3}\omega_{5j+4}],
\end{aligned} \tag{4.2}$$

and the equations for the decoupled variables ω_{5j} and ω_{5j+5} are given by,

$$\begin{aligned}
\dot{\omega}_{5j} &= -A_{5j+1}\omega_p\omega_{5j+1}, \\
\dot{\omega}_{5j+5} &= A_{5j+4}\omega_p\omega_{5j+4}.
\end{aligned}$$

The kinetic energy

$$\tilde{H}_j = \frac{1}{2} \left[\sum_{1 \leq l \leq 4} \frac{1}{|\hat{k} + (5j + l)p|^2} \omega_{5j+l}^2 + \frac{1}{|p|^2} \omega_p^2 \right],$$

and the enstrophy

$$\tilde{J}_2^{(j)} = \sum_{1 \leq l \leq 4} \omega_{5j+l}^2 + \omega_p^2,$$

are constants of motion for this system.

4.2 Perverted Heteroclinic Orbits When $\epsilon = 0$

From the studies in last subsection, the ($j = 0$) linearized system at the fixed point (3.7) has a quadruple of eigenvalues with nonzero real parts, and all ($j \neq 0$) linearized system at the fixed point (3.7) has two pairs of purely imaginary eigenvalues. Next we focus on the invariant subsystem (4.2) when $j = 0$, and generate explicit expressions for the unstable and stable manifolds of the line of fixed points (3.7). Notice that

$$A_1 = -\frac{3}{10}, \quad A_2 = \frac{1}{2}, \quad A_3 = A_2, \quad A_4 = A_1, \quad (4.3)$$

$$A_{1,2} = A_1 - A_2 = -\frac{4}{5}, \quad A_{2,3} = 0, \quad A_{3,4} = -A_{1,2};$$

then the invariant subsystem (4.2) for $j = 0$ can be rewritten as follows:

$$\begin{aligned} \dot{\omega}_1 &= -A_2 \omega_p \omega_2, \\ \dot{\omega}_2 &= A_1 \omega_p \omega_1 - A_2 \omega_p \omega_3, \\ \dot{\omega}_3 &= A_2 \omega_p \omega_2 - A_1 \omega_p \omega_4, \\ \dot{\omega}_4 &= A_2 \omega_p \omega_3, \\ \dot{\omega}_p &= A_{1,2} (\omega_3 \omega_4 - \omega_1 \omega_2), \end{aligned} \quad (4.4)$$

and the equations for the decoupled variables ω_0 and ω_5 are given by,

$$\begin{aligned} \dot{\omega}_0 &= -A_1 \omega_p \omega_1, \\ \dot{\omega}_5 &= A_1 \omega_p \omega_4. \end{aligned}$$

There are three invariants for the system (4.4):

$$I = 2A_{1,2}(\omega_1\omega_3 + \omega_2\omega_4) + A_2\omega_p^2, \quad (4.5)$$

$$U = A_1(\omega_1^2 + \omega_4^2) + A_2(\omega_2^2 + \omega_3^2), \quad (4.6)$$

$$J = \omega_p^2 + \omega_1^2 + \omega_2^2 + \omega_3^2 + \omega_4^2. \quad (4.7)$$

J is the enstrophy, and U is a linear combination of the kinetic energy and the enstrophy. I is an extra invariant which is peculiar to this invariant subsystem. With I , the explicit formula for the hyperbolic structure can be computed.

The common level set of these three invariants which is connected to the fixed point (3.7) determines the stable and unstable manifolds of the fixed point and its negative $-\omega^*$:

$$\omega_p = -\Gamma, \quad \omega_n = 0 \quad (n \in Z). \quad (4.8)$$

Using the polar coordinates:

$$\omega_1 = r \cos \theta, \quad \omega_4 = r \sin \theta; \quad \omega_2 = \rho \cos \vartheta, \quad \omega_3 = \rho \sin \vartheta;$$

we have the following explicit expressions for the stable and unstable manifolds of the fixed point (3.7) and its negative (4.8) represented through *perverted heteroclinic orbits*:

$$\begin{aligned}
\omega_p &= \Gamma \tanh \tau, \\
r &= \sqrt{\frac{A_2}{A_2 - A_1}} \Gamma \operatorname{sech} \tau, \\
\theta &= -\frac{A_2}{2\kappa} \ln \cosh \tau + \theta_0, \\
\rho &= \sqrt{\frac{-A_1}{A_2}} r, \\
\theta + \vartheta &= \begin{cases} -\arcsin \left[\frac{1}{2} \sqrt{\frac{A_2}{-A_1}} \right], & (\kappa > 0), \\ \pi + \arcsin \left[\frac{1}{2} \sqrt{\frac{A_2}{-A_1}} \right], & (\kappa < 0), \end{cases}
\end{aligned} \tag{4.9}$$

where A_1 and A_2 are given in (4.3), $\tau = \kappa\Gamma t + \tau_0$, (τ_0, θ_0) are the two parameters parametrizing the two-dimensional stable (unstable) manifold, and

$$\kappa = \sqrt{-A_1 A_2} \cos(\theta + \vartheta) = \pm \sqrt{-A_1 A_2} \sqrt{1 + \frac{A_2}{4A_1}}.$$

The two auxilliary variables ω_0 and ω_5 have the expressions:

$$\begin{aligned}
\omega_0 &= \frac{\alpha\beta}{1 + \beta^2} \operatorname{sech} \tau \left\{ \sin[\beta \ln \cosh \tau + \theta_0] - \frac{1}{\beta} \cos[\beta \ln \cosh \tau + \theta_0] \right\}, \\
\omega_5 &= \frac{\alpha\beta}{1 + \beta^2} \operatorname{sech} \tau \left\{ \cos[\beta \ln \cosh \tau + \theta_0] + \frac{1}{\beta} \sin[\beta \ln \cosh \tau + \theta_0] \right\},
\end{aligned}$$

where

$$\alpha = -A_1 \Gamma \kappa^{-1} \sqrt{\frac{A_2}{A_2 - A_1}}, \quad \beta = -\frac{A_2}{2\kappa}.$$

Remark 4.1 *In this remark, we will discuss the complex version of the system (4.4):*

$$\begin{aligned}
\dot{\omega}_1 &= -A_2 \bar{\omega}_p \omega_2, \\
\dot{\omega}_2 &= A_1 \omega_p \omega_1 - A_2 \bar{\omega}_p \omega_3, \\
\dot{\omega}_3 &= A_2 \omega_p \omega_2 - A_1 \bar{\omega}_p \omega_4, \\
\dot{\omega}_4 &= A_2 \omega_p \omega_3, \\
\dot{\omega}_p &= A_{1,2} (\bar{\omega}_3 \omega_4 - \bar{\omega}_1 \omega_2).
\end{aligned} \tag{4.10}$$

This is a ten dimensional Hamiltonian system with no reality restriction. For this system (4.10), we have one complex invariant

$$I_c = 2A_{1,2}(\bar{\omega}_1 \omega_3 + \bar{\omega}_2 \omega_4) + A_2 \omega_p^2,$$

and two real invariants

$$\begin{aligned} U_c &= A_1(|\omega_1|^2 + |\omega_4|^2) + A_2(|\omega_2|^2 + |\omega_3|^2), \\ J_c &= |\omega_p|^2 + |\omega_1|^2 + |\omega_2|^2 + |\omega_3|^2 + |\omega_4|^2. \end{aligned}$$

Thus, we have total four invariants which are not enough for the integrability of the Hamiltonian system (4.10). When we consider the reality restriction, we have three invariants. Their common level sets in the five dimensional real phase space, are two-dimensional. The stable and unstable manifolds of the fixed point are also two-dimensional, and these three invariants are enough to determine the stable and unstable manifolds.

4.3 Discussion on the Perverted Heteroclinic Orbits

The oscillatory nature of the heteroclinic orbit reflects the fact that the quadruple of eigenvalues with nonzero real parts, also has nonzero imaginary parts. The interesting nature of the heteroclinic orbits is that they all have a “perversion” which refers to the neighborhood of the turning point. The portions of the heteroclinic orbit in the neighborhoods of ω^* and $-\omega^*$ can be viewed as oriented helices. Then the entire heteroclinic orbit is a connection between a right-handed helix and a left-handed helix, and the connection part has to be a perversion. See Figure 4.1 for an illustration. From the study on the linearized 2D Euler equation [25], we realize that the eigenvalues of the fixed point ω^* only depend upon the modulus $|\omega_p|$ (the same fact is true for the dashed-line model too). Therefore, ω^* and $-\omega^*$ have the same eigenvalues. In fact, the eigenvalues appear in quadruples which make the connection of a right-handed helix with a left-handed helix feasible.

The term “perversion” was given by the 19th century topologist Listing to describe the spontaneous switching of a helical structure of one handedness to its mirror image. Tendril perversion in climbing plants had been described at length by Charles Darwin in his book [10]. Darwin interpreted the tendril perversion using the language of elasticity. Complete mathematical study on elastic filaments modelling tendril perversion has been developed by A. Goriely and M. Tabor [19] [13] [14] [15] [16] [18] [17]. Figure 4.2 shows a climbing plant with one tendril perversion [31]. One tendril can have many perversions [10], see Figure 4.3. Perversions can occur in problems like the microscopic properties of biological fibers such as cotton or the formation of bacterial macrofibers, telephone cords (Figure 4.2), false-twist technique in the textile industry etc. [19]. The explicit expression (4.9) of the perverted heteroclinic orbits shows that the unstable manifold $W^u(\omega^*)$ of the fixed point ω^* (3.7) is the same as the stable manifold $W^s(\omega^*)$ of the negative $-\omega^*$ (4.8) of ω^* , and the stable manifold of the fixed point ω^* (3.7) is the same as the unstable manifold of the negative $-\omega^*$ (4.8) of ω^* . Both $W^u(\omega^*)$ and $W^s(\omega^*)$ have the shapes of “painted eggs” (Figure 4.4). $W^u(\omega^*)$ and $W^s(\omega^*)$ together form the “lip” (Figure 4.4) which is a higher dimensional generalization of the heteroclinic connection on plane. As the first step toward understanding the degeneracy v.s. nondegeneracy nature of the hyperbolic structure of 2D Euler equation, we are interested in the ϵ -homotopy deformation of such hyperbolic structure for the dashed-line model. In the next section, we will use higher order Melnikov functions to study the “breaking” or “persistence” of such hyperbolic structure when ϵ is small.

Figure 4.1: The connection part of a right-handed helix and a left-handed helix has to be a perversion.

Figure 4.2: (a). Tendril perversion in *Bryonia dioica*. Illustration from Sachs' Text-book of Botany (1875); (b). Perversion in a telephone cord (Goriely and Tabor, 1997). The effect is achieved by fully stretching out and untwisting the cord and slowly bringing the ends together. The above figures are taken from Goriely and Tabor's papers (see References).

Figure 4.3: A caught tendril of *Bryonia dioica*, spirally contracted in reversed directions. Illustration from Darwin's book: *The Movements and Habits of Climbing Plants* (1875) (see References).

Figure 4.4: The unstable and stable manifolds of the fixed point ω^* (3.7): (a) and (b) show two “painted eggs” and (c) shows a “lip”.

5 The Higher Order Melnikov Functions

In this section, we are going to study the persistence of the hyperbolic structures given by (4.9), i.e., the persistence of the “painted eggs” and “lips” as shown in Figure 4.4 of the invariant subsystem (4.4) in the dashed-line model (3.13) when $\epsilon \neq 0$. We will use Melnikov functions to detect such persistence, and the Melnikov functions will be built upon the following two invariants of the dashed-line model (3.13) when $\epsilon = 0$, which are actually invariants of the invariant subsystem (4.4):

$$U = A_1(\omega_1^2 + \omega_4^2) + A_2(\omega_2^2 + \omega_3^2), \quad (5.1)$$

$$V = A_2(\omega_1^2 + \omega_2^2 + \omega_3^2 + \omega_4^2) - 2A_{1,2}(\omega_1\omega_3 + \omega_2\omega_4), \quad (5.2)$$

where V is a linear combination of the invariants I and J given in (4.5) and (4.7), $V = A_2J - I$.

From the spectral distribution Figure 3.5, when $\epsilon = 0$, the fixed point (3.7) or (4.8) has codimension 2 center-unstable and center-stable manifolds $W^{cu}(\pm\Gamma)$ and $W^{cs}(\pm\Gamma)$ under the flow (4.1), and the “painted eggs” are two-dimensional submanifolds of them. For sufficiently small ϵ , $W^{cu}(\pm\Gamma)$ and $W^{cs}(\pm\Gamma)$ perturb into $W_\epsilon^{cu}(\pm\Gamma)$ and $W_\epsilon^{cs}(\pm\Gamma)$. We are going to use the new notation

$$\omega = (\omega_p, \omega_n : n \in Z). \quad (5.3)$$

In this notation, we rewrite the dashed-line model (3.13) as follows:

$$\dot{\omega} = f(\omega) + \epsilon g(\omega). \quad (5.4)$$

Denote by $\omega^{(0)}$ the orbit given by (4.9) which solves the $\epsilon = 0$ form of (5.4):

$$\dot{\omega}^{(0)} = f(\omega^{(0)}). \quad (5.5)$$

5.1 The Melnikov Functions

The (first order) Melnikov functions are given by:

$$M_U = \int_{-\infty}^{\infty} \langle \nabla U, g \rangle |_{\omega^{(0)}} dt \quad (5.6)$$

$$\begin{aligned}
&= \int_{-\infty}^{\infty} [2A_0A_1\omega_p\omega_0\omega_1 - 2A_0A_1\omega_p\omega_4\omega_5]_{|\omega^{(0)}} dt \\
&= -2A_0 \int_{-\infty}^{\infty} [\omega_0^{(0)}\dot{\omega}_0^{(0)} + \omega_5^{(0)}\dot{\omega}_5^{(0)}] dt = 0, \\
M_V &= \int_{-\infty}^{\infty} \langle \nabla V, g \rangle_{|\omega^{(0)}} dt \\
&= \int_{-\infty}^{\infty} [2A_0A_2\omega_p\omega_0\omega_1 - 2A_0A_2\omega_p\omega_4\omega_5 \\
&\quad - 2A_0A_{1,2}\omega_p\omega_0\omega_3 + 2A_0A_{1,2}\omega_p\omega_2\omega_5]_{|\omega^{(0)}} dt \\
&= -2A_0 \int_{-\infty}^{\infty} \left[\frac{A_2}{A_1} (\omega_0^{(0)}\dot{\omega}_0^{(0)} + \omega_5^{(0)}\dot{\omega}_5^{(0)}) \right. \\
&\quad \left. + A_{1,2} (\omega_p^{(0)}\omega_0^{(0)}\omega_3^{(0)} - \omega_p^{(0)}\omega_2^{(0)}\omega_5^{(0)}) \right] dt = 0,
\end{aligned}$$

since the second round bracket is an odd function in τ . The above representations will be reproduced in the process of deriving higher order Melnikov functions in the next subsection. The above calculations show that the Melnikov functions are identically zero as functions of θ_0 and Γ . Thus the separation between $W_\epsilon^{cu}(\pm\Gamma)$ and $W_\epsilon^{cs}(\pm\Gamma)$ is at least of order $O(\epsilon^2)$. To further detect the separation between $W_\epsilon^{cu}(\pm\Gamma)$ and $W_\epsilon^{cs}(\pm\Gamma)$, we need to compute the second order Melnikov functions which are the leading order terms of the signed separation distances.

5.2 The Derivation of Higher Order Melnikov Functions

The derivation in this subsection is given without rigorous justifications, and rigorous justifications are future works.

Let $\omega^{(0)}(t)$ denote a heteroclinic orbit given by (4.9), and let Σ be a codimension 1 hypersurface which is transversal to the orbit $\omega^{(0)}(t)$ at $\omega^{(0)}(0)$. See Figure 5.1 on the setup of this derivation. Without loss of generality, we assume that in backward time $\omega^{(0)}(t)$ approaches ω^* (3.7) and in forward time $\omega^{(0)}(t)$ approaches $-\omega^*$ (4.8). The submanifolds $W_\epsilon^{cs}(-\Gamma) \cap \Sigma$ and $W_\epsilon^{cs}(\Gamma) \cap \Sigma$ have codimension 2 in Σ , and the codimensions are coordinated by ∇U and ∇V . Let $\omega^{(u)}(t, \epsilon)$ denote an orbit of the $(\epsilon \neq 0)$ system (3.13) which approaches ω^* in backward time. Let $\omega^{(u)}(0, \epsilon)$ be the intersection point of $\omega^{(u)}(t, \epsilon)$ with Σ . On the submanifold $W_\epsilon^{cs}(-\Gamma) \cap \Sigma$, let $\omega^{(s)}(0, \epsilon)$ be the point which has the same coordinates with $\omega^{(u)}(0, \epsilon)$ except the ∇U and ∇V directional coordinates in Σ . Denote by $\omega^{(s)}(t, \epsilon)$ the orbit of the $(\epsilon \neq 0)$ system (3.13) with initial point $\omega^{(s)}(0, \epsilon)$.

Define the signed distances:

$$\begin{aligned}
d_U &= \langle \nabla U(0), \omega^{(u)}(0, \epsilon) - \omega^{(s)}(0, \epsilon) \rangle \\
&= \langle \nabla U(0), \omega^{(u)}(0, \epsilon) - \omega^{(0)}(0) \rangle \\
&\quad - \langle \nabla U(0), \omega^{(s)}(0, \epsilon) - \omega^{(0)}(0) \rangle, \\
d_V &= \langle \nabla V(0), \omega^{(u)}(0, \epsilon) - \omega^{(s)}(0, \epsilon) \rangle \\
&= \langle \nabla V(0), \omega^{(u)}(0, \epsilon) - \omega^{(0)}(0) \rangle
\end{aligned} \tag{5.7}$$

Figure 5.1: The geometrical setup for deriving the second order Melnikov functions.

$$-\langle \nabla V(0), \omega^{(s)}(0, \epsilon) - \omega^{(0)}(0) \rangle. \quad (5.8)$$

From now on, we will do the derivation for d_U , and the derivation for d_V is the same. We define the following two functions:

$$\begin{aligned} \Delta_U^+(t, \epsilon) &= \langle \nabla U(t), \omega^{(s)}(t, \epsilon) - \omega^{(0)}(t) \rangle, \quad t \in [0, \infty), \\ \Delta_U^-(t, \epsilon) &= \langle \nabla U(t, \epsilon), \omega^{(u)}(t, \epsilon) - \omega^{(0)}(t) \rangle, \quad t \in (-\infty, 0], \end{aligned}$$

where $\nabla U(t) = \nabla U(\omega^{(0)}(t))$. Then

$$d_U = \Delta_U^-(0, \epsilon) - \Delta_U^+(0, \epsilon). \quad (5.9)$$

Next we will do the derivation for $\Delta_U^+(t, \epsilon)$ and the derivation for $\Delta_U^-(t, \epsilon)$ is the same. For any $T > 0$, $\Delta_U^+(t, \epsilon)$ as a function of ϵ has the Taylor expansion:

$$\Delta_U^+(t, \epsilon) = \sum_{n=1}^{\infty} \epsilon^n \Delta_U^{(+,n)}(t), \quad t \in [0, T], \quad (5.10)$$

where

$$\Delta_U^{(+,n)}(t) = \frac{1}{n!} \frac{\partial^n}{\partial \epsilon^n} \Delta_U^+(t, 0) = \frac{1}{n!} \langle \nabla U(t), \frac{\partial^n}{\partial \epsilon^n} \omega^{(s)}(t, 0) \rangle; \quad (5.11)$$

and $\omega^{(s)}(t, \epsilon)$ as a function of ϵ has the Taylor expansion:

$$\omega^{(s)}(t, \epsilon) = \omega^{(0)}(t) + \sum_{n=1}^{\infty} \epsilon^n \omega^{(s,n)}(t), \quad t \in [0, T], \quad (5.12)$$

where

$$\omega^{(s,n)}(t) = \frac{1}{n!} \frac{\partial^n}{\partial \epsilon^n} \omega^{(s)}(t, 0). \quad (5.13)$$

The function $\omega^{(s,n)}$ satisfies the equation:

$$\dot{\omega}^{(s,n)} = \nabla f(\omega^{(0)}) \circ \omega^{(s,n)} + h^{(s,n)}, \quad t \in [0, T], \quad (5.14)$$

where

$$h^{(s,n)} = \frac{1}{n!} \left(\frac{\partial^n}{\partial \epsilon^n} \left[f(\omega^{(s)}(t, \epsilon)) + \epsilon g(\omega^{(s)}(t, \epsilon)) \right] \right)_{\epsilon=0} - \nabla f(\omega^{(0)}) \circ \omega^{(s,n)},$$

for example

$$\begin{aligned}
h^{(s,1)} &= g(\omega^{(0)}) , \\
h^{(s,2)} &= \frac{1}{2} \left\{ \nabla^2 f(\omega^{(0)}) \circ \omega^{(s,1)} \right\} \circ \omega^{(s,1)} \\
&\quad + \nabla g(\omega^{(0)}) \circ \omega^{(s,1)} , \\
h^{(s,3)} &= \left\{ \nabla^2 f(\omega^{(0)}) \circ \omega^{(s,1)} \right\} \circ \omega^{(s,2)} \\
&\quad + \frac{1}{6} \left\{ \left\{ \nabla^3 f(\omega^{(0)}) \circ \omega^{(s,1)} \right\} \circ \omega^{(s,1)} \right\} \circ \omega^{(s,1)} \\
&\quad + \nabla g(\omega^{(0)}) \circ \omega^{(s,2)} \\
&\quad + \frac{1}{2} \left\{ \nabla^2 g(\omega^{(0)}) \circ \omega^{(s,1)} \right\} \circ \omega^{(s,1)} .
\end{aligned}$$

Next we are going to derive an expression for the time derivative of the functions $\Delta_U^{(+,n)}$.

$$\begin{aligned}
\dot{\Delta}_U^{(+,n)} &= \langle \nabla^2 U \circ \dot{\omega}^{(0)} , \omega^{(s,n)} \rangle + \langle \nabla U , \dot{\omega}^{(s,n)} \rangle \\
&= \langle \nabla^2 U \circ f , \omega^{(s,n)} \rangle + \langle \nabla U , \nabla f \circ \omega^{(s,n)} \rangle + \langle \nabla U , h^{(s,n)} \rangle .
\end{aligned} \tag{5.15}$$

Notice that

$$\langle \nabla U , f \rangle = 0 , \tag{5.16}$$

from the invariance of U under the $\epsilon = 0$ flow (4.1); then the variation of the equation (5.16) leads to:

$$\langle \nabla^2 U \circ \delta\omega , f \rangle + \langle \nabla U , \nabla f \circ \delta\omega \rangle = 0 ,$$

and since $\nabla^2 U$ is a symmetric operator, we have

$$\langle \nabla^2 U \circ f , \delta\omega \rangle + \langle \nabla U , \nabla f \circ \delta\omega \rangle = 0 . \tag{5.17}$$

If we substitute $\delta\omega$ in (5.17) by $\omega^{(s,n)}$, we see that equation (5.15) is reduced to

$$\dot{\Delta}_U^{(+,n)} = \langle \nabla U , h^{(s,n)} \rangle , \quad t \in [0, T] . \tag{5.18}$$

Without rigorous justifications and taking the limit $T \rightarrow +\infty$ in (5.18), we have

$$\Delta_U^{(+,n)}(0) = - \int_0^\infty \langle \nabla U(\omega^{(0)}) , h^{(s,n)} \rangle dt . \tag{5.19}$$

Similarly,

$$\Delta_U^{(-,n)}(0) = \int_{-\infty}^0 \langle \nabla U(\omega^{(0)}) , h^{(u,n)} \rangle dt , \tag{5.20}$$

where $h^{(u,n)}$ has the same expression as $h^{(s,n)}$ with s replaced by u everywhere,

$$\begin{aligned}
\Delta_{\bar{U}}(t, \epsilon) &= \sum_{n=1}^{\infty} \epsilon^n \Delta_U^{(-,n)}(t) , \quad t \in (-\infty, 0] , \\
\Delta_U^{(-,n)}(t) &= \frac{1}{n!} \frac{\partial^n}{\partial \epsilon^n} \Delta_{\bar{U}}(t, 0)
\end{aligned} \tag{5.21}$$

$$= \frac{1}{n!} \langle \nabla U(t), \frac{\partial^n}{\partial \epsilon^n} \omega^{(u)}(t, 0) \rangle, \quad (5.22)$$

$$\omega^{(u)}(t, \epsilon) = \omega^{(0)}(t) + \sum_{n=1}^{\infty} \epsilon^n \omega^{(u,n)}(t), \quad t \in (-\infty, 0], \quad (5.23)$$

$$\omega^{(u,n)}(t) = \frac{1}{n!} \frac{\partial^n}{\partial \epsilon^n} \omega^{(u)}(t, 0), \quad (5.24)$$

$$\dot{\omega}^{(u,n)} = \nabla f(\omega^{(0)}) \circ \omega^{(u,n)} + h^{(u,n)}, \quad t \in (-\infty, 0]. \quad (5.25)$$

From the expression (5.9) of the signed distance d_U , we have

$$\begin{aligned} d_U &= \sum_{n=1}^{\infty} \epsilon^n \left[\Delta_U^{(-,n)}(0) - \Delta_U^{(+,n)}(0) \right] \\ &= \sum_{n=1}^{\infty} \epsilon^n M_U^{(n)}, \end{aligned}$$

where $M_U^{(n)}$ is called the n -th order Melnikov function and $M_U^{(1)}$ is the usual Melnikov function.

Notice that $\omega^{(u)}(0, \epsilon)$ and $\omega^{(s)}(0, \epsilon)$ are chosen to have the same coordinates except the $\nabla U(0)$ and $\nabla V(0)$ directions. From the expressions (5.10) (5.11) (5.12) (5.13) (5.21) (5.22) (5.23) and (5.24), if $M_Y^{(j)} \equiv 0$, $j = 1, 2, \dots, n-1$; $Y = U, V$; then

$$\omega^{(s,j)}(0) = \omega^{(u,j)}(0), \quad j = 1, 2, \dots, n-1.$$

Notice that both $\omega^{(s,j)}$ and $\omega^{(u,j)}$ satisfy the same form of equations (5.14) and (5.25); thus $\omega^{(s,j)}$ and $\omega^{(u,j)}$ together represent one solution on the entire interval $t \in (-\infty, \infty)$, and we can drop 's' and 'u', and use the simple notation $\omega^{(j)}$ for $j = 1, 2, \dots, n-1$.

$$\dot{\omega}^{(j)} = \nabla f(\omega^{(0)}) \circ \omega^{(j)} + h^{(j)}, \quad t \in (-\infty, \infty), \quad (5.26)$$

$$j = 1, 2, \dots, n-1,$$

where

$$\begin{aligned} h^{(j)} &= \frac{1}{j!} \left(\frac{\partial^j}{\partial \epsilon^j} \left[f(\omega^{(s)}(t, \epsilon)) + \epsilon g(\omega^{(s)}(t, \epsilon)) \right] \right)_{\epsilon=0} \\ &\quad - \nabla f(\omega^{(0)}) \circ \omega^{(j)}, \end{aligned} \quad (5.27)$$

$$j = 1, 2, \dots, n,$$

for example

$$\begin{aligned} h^{(1)} &= g(\omega^{(0)}), \\ h^{(2)} &= \frac{1}{2} \left\{ \nabla^2 f(\omega^{(0)}) \circ \omega^{(1)} \right\} \circ \omega^{(1)} \\ &\quad + \nabla g(\omega^{(0)}) \circ \omega^{(1)}, \end{aligned}$$

$$\begin{aligned}
h^{(3)} &= \left\{ \nabla^2 f(\omega^{(0)}) \circ \omega^{(1)} \right\} \circ \omega^{(2)} \\
&+ \frac{1}{6} \left\{ \left\{ \nabla^3 f(\omega^{(0)}) \circ \omega^{(1)} \right\} \circ \omega^{(1)} \right\} \circ \omega^{(1)} \\
&+ \nabla g(\omega^{(0)}) \circ \omega^{(2)} \\
&+ \frac{1}{2} \left\{ \nabla^2 g(\omega^{(0)}) \circ \omega^{(1)} \right\} \circ \omega^{(1)} .
\end{aligned}$$

Notice that both $\omega^{(u)}(t, \epsilon)$ and $\omega^{(0)}(t)$ approach the same point $-\omega^*$ in backward time, we have

$$\omega^{(u,l)}(-\infty) = 0, \quad \forall l = 1, 2, \dots . \quad (5.28)$$

From the expressions (5.19) and (5.20), we have

$$M_U^{(n)} = \int_{-\infty}^{\infty} \langle \nabla U(\omega^{(0)}), h^{(n)} \rangle dt,$$

similarly for $M_V^{(n)}$.

Summary. *The signed distances d_Y ($Y = U, V$) defined in (5.7) and (5.8) have the representations:*

$$d_Y = \sum_{n=1}^{\infty} \epsilon^n M_Y^{(n)}, \quad (Y = U, V). \quad (5.29)$$

If $M_Y^{(j)} \equiv 0$, $j = 1, 2, \dots, n-1$; $Y = U, V$; then

$$M_Y^{(n)} = \int_{-\infty}^{\infty} \langle \nabla Y(\omega^{(0)}), h^{(n)} \rangle dt, \quad Y = U, V;$$

where $h^{(n)}$ is given in (5.27) and $\omega^{(j)}$ ($j = 1, 2, \dots, n-1$) solves the linear equation (5.26) under the boundary condition (5.28).

5.3 Numerical Evaluations of the Second and Third Order Melnikov Functions

5.3.1 Numerical Evaluations of the Second Order Melnikov Functions

In the formulae of the second order Melnikov functions [(5.29), for $n = 2$], since the functions U and V only depend on ω_j ($1 \leq j \leq 4$), only the following four components of $h^{(2)}$ enter the evaluation:

$$h_1^{(2)} = -A_2 \omega_p^{(1)} \omega_2^{(1)} + A_0 [\omega_p^{(0)} \omega_0^{(1)} + \omega_p^{(1)} \omega_0^{(0)}], \quad (5.30)$$

$$h_2^{(2)} = A_1 \omega_p^{(1)} \omega_1^{(1)} - A_2 \omega_p^{(1)} \omega_3^{(1)}, \quad (5.31)$$

$$h_3^{(2)} = A_2 \omega_p^{(1)} \omega_2^{(1)} - A_1 \omega_p^{(1)} \omega_4^{(1)}, \quad (5.32)$$

$$h_4^{(2)} = A_2 \omega_p^{(1)} \omega_3^{(1)} - A_0 [\omega_p^{(0)} \omega_5^{(1)} + \omega_p^{(1)} \omega_5^{(0)}]. \quad (5.33)$$

Thus we need to know the functions $\omega_p^{(1)}, \omega_j^{(1)}$ ($0 \leq j \leq 5$). Specifically these functions satisfy a set of decoupled systems of linear equations. The five functions $\omega_p^{(1)}, \omega_\ell^{(1)}$ ($1 \leq \ell \leq 4$) satisfy a self-contained system of linear equations with variable coefficients:

$$\begin{pmatrix} \omega_1^{(1)} \\ \omega_2^{(1)} \\ \omega_3^{(1)} \\ \omega_4^{(1)} \\ \omega_p^{(1)} \end{pmatrix} = \mathcal{A} \begin{pmatrix} \omega_1^{(1)} \\ \omega_2^{(1)} \\ \omega_3^{(1)} \\ \omega_4^{(1)} \\ \omega_p^{(1)} \end{pmatrix} + \mathcal{B}, \quad (5.34)$$

where

$$\mathcal{A} = \begin{pmatrix} 0 & -A_2\omega_p^{(0)} & 0 & 0 & -A_2\omega_2^{(0)} \\ A_1\omega_p^{(0)} & 0 & -A_2\omega_p^{(0)} & 0 & A_1\omega_1^{(0)} - A_2\omega_3^{(0)} \\ 0 & A_2\omega_p^{(0)} & 0 & -A_1\omega_p^{(0)} & A_2\omega_2^{(0)} - A_1\omega_4^{(0)} \\ 0 & 0 & A_2\omega_p^{(0)} & 0 & A_2\omega_3^{(0)} \\ -A_{1,2}\omega_2^{(0)} & -A_{1,2}\omega_1^{(0)} & A_{1,2}\omega_4^{(0)} & A_{1,2}\omega_3^{(0)} & 0 \end{pmatrix},$$

$$\mathcal{B} = \begin{pmatrix} A_0\omega_p^{(0)}\omega_0^{(0)} \\ 0 \\ 0 \\ -A_0\omega_p^{(0)}\omega_5^{(0)} \\ -A_{4,5}\omega_4^{(0)}\omega_5^{(0)} - A_{0,1}\omega_0^{(0)}\omega_1^{(0)} \end{pmatrix}.$$

The functions $\omega_0^{(1)}$ and $\omega_5^{(1)}$ satisfy the linear equations:

$$\dot{\omega}_0^{(1)} = \omega_p^{(0)}[A_{-1}\omega_{-1}^{(1)} - A_1\omega_1^{(1)}] - A_1\omega_1^{(0)}\omega_p^{(1)}, \quad (5.35)$$

$$\dot{\omega}_5^{(1)} = \omega_p^{(0)}[A_4\omega_4^{(1)} - A_6\omega_6^{(1)}] + A_4\omega_4^{(0)}\omega_p^{(1)}. \quad (5.36)$$

The two functions $\omega_{-1}^{(1)}$ and $\omega_6^{(1)}$ on the right hand sides of (5.35) and (5.36) are obtained from solving the following two self-contained systems of linear equations:

$$\frac{d}{d\zeta} \begin{bmatrix} \omega_{-1}^{(1)} \\ \omega_{-2}^{(1)} \\ \omega_{-3}^{(1)} \\ \omega_{-4}^{(1)} \end{bmatrix} = \mathcal{C} \begin{bmatrix} \omega_{-1}^{(1)} \\ \omega_{-2}^{(1)} \\ \omega_{-3}^{(1)} \\ \omega_{-4}^{(1)} \end{bmatrix} + \mathcal{D}, \quad (5.37)$$

$$\frac{d}{d\zeta} \begin{bmatrix} \omega_6^{(1)} \\ \omega_7^{(1)} \\ \omega_8^{(1)} \\ \omega_9^{(1)} \end{bmatrix} = \mathcal{E} \begin{bmatrix} \omega_6^{(1)} \\ \omega_7^{(1)} \\ \omega_8^{(1)} \\ \omega_9^{(1)} \end{bmatrix} + \mathcal{F}, \quad (5.38)$$

where $\frac{d}{d\zeta} = \frac{1}{\omega_p^{(0)}} \frac{d}{dt}$, $\zeta = \frac{1}{\kappa} \ln \cosh(\kappa\Gamma t + \tau_0)$,

$$\begin{aligned} \mathcal{C} &= \begin{bmatrix} 0 & A_{-2} & 0 & 0 \\ -A_{-1} & 0 & A_{-3} & 0 \\ 0 & -A_{-2} & 0 & A_{-4} \\ 0 & 0 & -A_{-3} & 0 \end{bmatrix} \\ &= \begin{bmatrix} 0 & -\frac{39}{82} & 0 & 0 \\ \frac{23}{50} & 0 & -\frac{59}{122} & 0 \\ 0 & \frac{39}{82} & 0 & -\frac{83}{170} \\ 0 & 0 & \frac{59}{122} & 0 \end{bmatrix}, \\ \mathcal{D} &= \begin{bmatrix} -A_0\omega_0^{(0)} \\ 0 \\ 0 \\ 0 \end{bmatrix} = \begin{bmatrix} \frac{11}{26}\omega_0^{(0)} \\ 0 \\ 0 \\ 0 \end{bmatrix}. \\ \mathcal{E} &= \begin{bmatrix} 0 & -A_7 & 0 & 0 \\ A_6 & 0 & -A_8 & 0 \\ 0 & A_7 & 0 & -A_9 \\ 0 & 0 & A_8 & 0 \end{bmatrix} = -\mathcal{C}, \\ \mathcal{F} &= \begin{bmatrix} A_5\omega_5^{(0)} \\ 0 \\ 0 \\ 0 \end{bmatrix} = \begin{bmatrix} -\frac{11}{26}\omega_5^{(0)} \\ 0 \\ 0 \\ 0 \end{bmatrix}. \end{aligned}$$

The characteristic equation for the matrix \mathcal{C} :

$$\lambda^4 + \lambda^2 \left[\frac{23 \times 39}{50 \times 82} + \frac{59}{122} \left(\frac{39}{82} + \frac{83}{170} \right) \right] + \frac{23 \times 39 \times 59 \times 83}{50 \times 82 \times 122 \times 170} = 0,$$

has only imaginary eigenvalues,

$$\lambda_{1,2} \doteq \pm i 0.773, \quad \lambda_{3,4} \doteq \pm i 0.295.$$

Let v_j ($1 \leq j \leq 4$) be the corresponding eigenvectors, $v = \text{columns } \{v_1, v_2, v_3, v_4\}$, $w^- = (\omega_{-1}^{(1)}, \omega_{-2}^{(1)}, \omega_{-3}^{(1)}, \omega_{-4}^{(1)})^T$, and $w^+ = (\omega_6^{(1)}, \omega_7^{(1)}, \omega_8^{(1)}, \omega_9^{(1)})^T$; then

$$w^-(\zeta) = v \int_{\text{sign}(\kappa)\infty}^{\zeta} \text{diag} \left\{ e^{\lambda_1(\zeta-\xi)}, e^{\lambda_2(\zeta-\xi)}, e^{\lambda_3(\zeta-\xi)}, e^{\lambda_4(\zeta-\xi)} \right\} v^{-1} \mathcal{D}(\xi) d\xi, \quad (5.39)$$

$$w^+(\zeta) = v \int_{\text{sign}(\kappa)\infty}^{\zeta} \text{diag} \left\{ e^{\lambda_1(\xi-\zeta)}, e^{\lambda_2(\xi-\zeta)}, e^{\lambda_3(\xi-\zeta)}, e^{\lambda_4(\xi-\zeta)} \right\} v^{-1} \mathcal{F}(\xi) d\xi. \quad (5.40)$$

The solutions w^\pm given above satisfy the boundary condition $w^\pm(t = -\infty) = 0$. In fact, w^\pm vanish at both positive and negative infinities, $w^\pm(t = \infty) = 0$.

The system of coupled linear equations (5.34), (5.37) and (5.38) were integrated numerically by Thomas Witelski using a fourth order Runge-Kutta scheme. The resulting numerical solutions were then used to evaluate the integrals for the second order Melnikov function $M_U^{(2)}$ and $M_V^{(2)}$ using the trapezoidal rule. For calculations with sufficiently small step-sizes, the second order Melnikov functions were found to be identically zero to machine precision, independent of the value of the parameters θ_0 and τ_0 . Evaluation of the partial integrals for $-\infty < \tau \leq t$ strongly suggest that the integrands of $M_U^{(2)}$ and $M_V^{(2)}$ are odd functions.

5.3.2 Numerical Evaluations of the Third Order Melnikov Functions

In the formulae of the third order Melnikov functions [(5.29), for $n = 3$], since the functions U and V only depend on ω_j ($1 \leq j \leq 4$), only the following four components of $h^{(3)}$ enter the evaluation:

$$\begin{aligned} h_1^{(3)} &= \left[A_0 \omega_p^{(0)} \right] \omega_0^{(2)} - \left[A_2 \omega_p^{(1)} \right] \omega_2^{(2)} \\ &\quad + \left[A_0 \omega_0^{(0)} - A_2 \omega_2^{(1)} \right] \omega_p^{(2)} + \left[A_0 \omega_0^{(1)} \omega_p^{(1)} \right], \\ h_2^{(3)} &= \left[A_1 \omega_p^{(1)} \right] \omega_1^{(2)} - \left[A_2 \omega_p^{(1)} \right] \omega_3^{(2)} \\ &\quad + \left[A_1 \omega_1^{(1)} - A_2 \omega_3^{(1)} \right] \omega_p^{(2)}, \\ h_3^{(3)} &= \left[A_2 \omega_p^{(1)} \right] \omega_2^{(2)} - \left[A_1 \omega_p^{(1)} \right] \omega_4^{(2)} \\ &\quad + \left[A_2 \omega_2^{(1)} - A_1 \omega_4^{(1)} \right] \omega_p^{(2)}, \\ h_4^{(3)} &= \left[A_2 \omega_p^{(1)} \right] \omega_3^{(2)} - \left[A_5 \omega_p^{(0)} \right] \omega_5^{(2)} \\ &\quad + \left[A_2 \omega_3^{(1)} - A_5 \omega_5^{(0)} \right] \omega_p^{(2)} - \left[A_5 \omega_5^{(1)} \omega_p^{(1)} \right]. \end{aligned}$$

Thus we need to know the functions $\omega_p^{(2)}$, $\omega_j^{(2)}$ ($0 \leq j \leq 5$). Specifically these functions satisfy a set of decoupled systems of linear equations. The five functions $\omega_p^{(2)}$, $\omega_\ell^{(2)}$ ($1 \leq$

$\ell \leq 4$) satisfy a self-contained system of linear equations with variable coefficients:

$$\begin{pmatrix} \omega_1^{(2)} \\ \omega_2^{(2)} \\ \omega_3^{(2)} \\ \omega_4^{(2)} \\ \omega_p^{(2)} \end{pmatrix} = \mathcal{A} \begin{pmatrix} \omega_1^{(2)} \\ \omega_2^{(2)} \\ \omega_3^{(2)} \\ \omega_4^{(2)} \\ \omega_p^{(2)} \end{pmatrix} + \mathcal{B}^{(2)},$$

where \mathcal{A} is given in (5.34), and

$$\mathcal{B}^{(2)} = \begin{pmatrix} h_1^{(2)} \\ h_2^{(2)} \\ h_3^{(2)} \\ h_4^{(2)} \\ h_p^{(2)} \end{pmatrix},$$

where $h_1^{(2)}$, $h_2^{(2)}$, $h_3^{(2)}$ and $h_4^{(2)}$ are given in (5.30), (5.31), (5.32) and (5.33), and

$$\begin{aligned} h_p^{(2)} = & - \left[A_{-4,-3} \omega_{-4}^{(1)} \omega_{-3}^{(1)} + A_{-3,-2} \omega_{-3}^{(1)} \omega_{-2}^{(1)} + A_{-2,-1} \omega_{-2}^{(1)} \omega_{-1}^{(1)} \right. \\ & + A_{-1,0} \omega_{-1}^{(1)} \omega_0^{(0)} + A_{0,1} (\omega_0^{(0)} \omega_1^{(1)} + \omega_0^{(1)} \omega_1^{(0)}) \\ & + A_{1,2} \omega_1^{(1)} \omega_2^{(1)} + A_{2,3} \omega_2^{(1)} \omega_3^{(1)} + A_{3,4} \omega_3^{(1)} \omega_4^{(1)} \\ & + A_{4,5} (\omega_4^{(0)} \omega_5^{(1)} + \omega_4^{(1)} \omega_5^{(0)}) + A_{5,6} \omega_5^{(0)} \omega_6^{(1)} \\ & \left. + A_{6,7} \omega_6^{(1)} \omega_7^{(1)} + A_{7,8} \omega_7^{(1)} \omega_8^{(1)} + A_{8,9} \omega_8^{(1)} \omega_9^{(1)} \right]. \end{aligned}$$

This expression is obtained from the fact that $\omega_l^{(1)} = 0$ for $l < -5$ and $l > 10$. The two functions $\omega_0^{(2)}$ and $\omega_5^{(2)}$ satisfy the linear equations:

$$\dot{\omega}_0^{(2)} = \left[A_{-1} \omega_p^{(0)} \right] \omega_{-1}^{(2)} - \left[A_1 \omega_p^{(0)} \right] \omega_1^{(2)} - \left[A_1 \omega_1^{(0)} \right] \omega_p^{(2)} + h_0^{(2)}, \quad (5.41)$$

$$\dot{\omega}_5^{(2)} = \left[A_4 \omega_p^{(0)} \right] \omega_4^{(2)} + \left[A_4 \omega_4^{(0)} \right] \omega_p^{(2)} - \left[A_6 \omega_p^{(0)} \right] \omega_6^{(2)} + h_5^{(2)}, \quad (5.42)$$

where

$$\begin{aligned} h_0^{(2)} &= A_{-1} \omega_p^{(1)} \omega_{-1}^{(1)} - A_1 \omega_p^{(1)} \omega_1^{(1)}, \\ h_5^{(2)} &= A_4 \omega_p^{(1)} \omega_4^{(1)} - A_6 \omega_p^{(1)} \omega_6^{(1)}. \end{aligned}$$

The two functions $\omega_{-1}^{(2)}$ and $\omega_6^{(2)}$ on the right hand sides of (5.41) and (5.42) are obtained from solving the following two self-contained systems of linear equations:

$$\frac{d}{d\zeta} \begin{bmatrix} \omega_{-1}^{(2)} \\ \omega_{-2}^{(2)} \\ \omega_{-3}^{(2)} \\ \omega_{-4}^{(2)} \end{bmatrix} = \mathcal{C} \begin{bmatrix} \omega_{-1}^{(2)} \\ \omega_{-2}^{(2)} \\ \omega_{-3}^{(2)} \\ \omega_{-4}^{(2)} \end{bmatrix} + \mathcal{D}^{(2)}, \quad (5.43)$$

$$\frac{d}{d\zeta} \begin{bmatrix} \omega_6^{(2)} \\ \omega_7^{(2)} \\ \omega_8^{(2)} \\ \omega_9^{(2)} \end{bmatrix} = \mathcal{E} \begin{bmatrix} \omega_6^{(2)} \\ \omega_7^{(2)} \\ \omega_8^{(2)} \\ \omega_9^{(2)} \end{bmatrix} + \mathcal{F}^{(2)}, \quad (5.44)$$

where ζ , \mathcal{C} and \mathcal{E} are given in (5.37) and (5.38),

$$\mathcal{D}^{(2)} = \frac{1}{\omega_p^{(0)}} \begin{bmatrix} h_{-1}^{(2)} \\ h_{-2}^{(2)} \\ h_{-3}^{(2)} \\ h_{-4}^{(2)} \end{bmatrix}, \quad \mathcal{F}^{(2)} = \frac{1}{\omega_p^{(0)}} \begin{bmatrix} h_6^{(2)} \\ h_7^{(2)} \\ h_8^{(2)} \\ h_9^{(2)} \end{bmatrix},$$

$$\begin{aligned} h_{-1}^{(2)} &= A_{-2}\omega_p^{(1)}\omega_{-2}^{(1)} - A_0(\omega_p^{(0)}\omega_0^{(1)} + \omega_p^{(1)}\omega_0^{(0)}), \\ h_{-2}^{(2)} &= A_{-3}\omega_p^{(1)}\omega_{-3}^{(1)} - A_{-1}\omega_p^{(1)}\omega_{-1}^{(1)}, \\ h_{-3}^{(2)} &= A_{-4}\omega_p^{(1)}\omega_{-4}^{(1)} - A_{-2}\omega_p^{(1)}\omega_{-2}^{(1)}, \\ h_{-4}^{(2)} &= A_{-5}\omega_p^{(0)}\omega_{-5}^{(1)} - A_{-3}\omega_p^{(1)}\omega_{-3}^{(1)}, \\ h_6^{(2)} &= A_5(\omega_p^{(0)}\omega_5^{(1)} + \omega_p^{(1)}\omega_5^{(0)}) - A_7\omega_p^{(1)}\omega_7^{(1)}, \\ h_7^{(2)} &= A_6\omega_p^{(1)}\omega_6^{(1)} - A_8\omega_p^{(1)}\omega_8^{(1)}, \\ h_8^{(2)} &= A_7\omega_p^{(1)}\omega_7^{(1)} - A_9\omega_p^{(1)}\omega_9^{(1)}, \\ h_9^{(2)} &= A_8\omega_p^{(1)}\omega_8^{(1)} - A_{10}\omega_p^{(0)}\omega_{10}^{(1)}. \end{aligned}$$

In these formulas, $\omega_{-5}^{(1)}$ and $\omega_{10}^{(1)}$ appeared, and they can be obtained from,

$$\begin{cases} \dot{\omega}_{-5}^{(1)} = -A_{-4}\omega_p^{(0)}\omega_{-4}^{(1)}, \\ \dot{\omega}_{10}^{(1)} = A_9\omega_p^{(0)}\omega_9^{(1)}. \end{cases}$$

Let $\hat{w}^- = (\omega_{-1}^{(2)}, \omega_{-2}^{(2)}, \omega_{-3}^{(2)}, \omega_{-4}^{(2)})^T$, and $\hat{w}^+ = (\omega_6^{(2)}, \omega_7^{(2)}, \omega_8^{(2)}, \omega_9^{(2)})^T$; then we have the similar representations as for w^- and w^+ ,

$$\hat{w}^-(\zeta) = v \int_{\text{sign}(\kappa)\infty}^{\zeta} \text{diag} \left\{ e^{\lambda_1(\zeta-\xi)}, e^{\lambda_2(\zeta-\xi)}, e^{\lambda_3(\zeta-\xi)}, e^{\lambda_4(\zeta-\xi)} \right\}$$

$$v^{-1}\mathcal{D}^{(2)}(\xi) d\xi , \tag{5.45}$$

$$\hat{w}^+(\zeta) = v \int_{\text{sign}(\kappa)\infty}^{\zeta} \text{diag} \left\{ e^{\lambda_1(\xi-\zeta)}, e^{\lambda_2(\xi-\zeta)}, e^{\lambda_3(\xi-\zeta)}, e^{\lambda_4(\xi-\zeta)} \right\} v^{-1}\mathcal{F}^{(2)}(\xi) d\xi . \tag{5.46}$$

The solutions \hat{w}^\pm given above satisfy the boundary condition $\hat{w}^\pm(t = -\infty) = 0$. In fact, \hat{w}^\pm vanish at both positive and negative infinities, $\hat{w}^\pm(t = \infty) = 0$.

The above systems are solved under the boundary condition,

$$\omega_l^{(2)}(t = -\infty) = 0 , \quad \forall l \in Z .$$

Moreover, direct verification shows that $\omega_l^{(2)} = 0$ for $l < -10$ and $l > 15$. For this case, the numerics of Thomas Witelski could not give a firm conclusion, and we are continuing investigating the numerics. This numerics is a part of a future project on numerical investigation of the degeneracy v.s. nondegeneracy of the hyperbolic foliations of the 2D Euler equation.

6 Conclusion and Discussion

In this Part II of our study, we see an explicit representation for the degeneracy of the hyperbolic structures for a Galerkin truncation. We use higher order Melnikov functions to study the robustness of such structures for the so-called dashed-line model. We find that both the first and the second order Melnikov functions are identically zero, which indicates that such structures are relatively robust. The study in this paper serves as a clue in searching for homoclinic structures for 2D Euler equation. The recent breakthrough result [24] of mine on the existence of a Lax pair for 2D Euler equation makes it plausible for the existence of homoclinic structures.

Acknowledgment: The author is greatly indebted for the numerical contribution of Professor Thomas Witelski. The work of Thomas was carried at MIT and Duke University. The author was surprised in finding out that Thomas did not want to be a co-author, rather gave all the credits to the author.

References

- [1] V. I. Arnold. Sur la Geometrie Differentielle des Groupes de Lie de Dimension Infinie et ses Applications a L'hydrodynamique des Fluides Parfaits. *Ann. Inst. Fourier, Grenoble*, 16,1:319–361, 1966.
- [2] R. Beals and R. R. Coifman. Linear Spectral Problems, Non-linear Equations and the $\bar{\partial}$ -Method. *Inverse Problems*, 5:87–130, 1989.
- [3] L. Biferale, A. Lambert, R. Lima, and G. Paladin. Transition to Chaos in a Shell Model of Turbulence. *Physica D*, 80:105–119, 1995.
- [4] S. Childress. *personal communication*, 2000.
- [5] S.-N. Chow and M. Yamashita. Geometry of the Melnikov Vector. *Nonlinear Equations in the Applied Sciences, Math. Sci. Engrg.*, 185:79–148, 1992.
- [6] W. Craig. Birkhoff Normal Forms for Water Waves. *Contemporary Mathematics*, 200:57–74, 1996.
- [7] W. Craig and M. Groves. Normal Forms for Water Motion in Fluid Interfaces. *Preprint*, 1997.
- [8] W. Craig and P. A. Worfolk. An Integrable Normal Form for Water Waves in Infinite Depth. *Physica D*, 84:513–531, 1995.
- [9] H. Dankowicz. Looking for Chaos. An Extension and Alternative to Melnikov's Method. *Internat. J. Bifur. Chaos Appl. Sci. Engrg.*, 6, no.3:485–496, 1996.
- [10] C. Darwin. *The Movements and Habits of Climbing Plants*. London: John Murray, 1975.
- [11] A. Fokas and M. J. Ablowitz. The Inverse Scattering Transform for Multidimensional (2+1) Problems. *Lecture Notes in Physics, Springer, Berlin-NY*, 189:137–183, 1983.
- [12] V. G. Gelfreich. Melnikov Method and Exponentially Small Splitting of Separatrices. *Physica D*, 101:227–248, 1997.
- [13] A. Goriely and M. Tabor. New Amplitude Equations for Thin Elastic Rods. *Phys. Rev. Lett.*, 77, No. 17:3537–3540, 1996.
- [14] A. Goriely and M. Tabor. Nonlinear Dynamics of Filaments I. Dynamical Instabilities. *Physica D*, 105:20–44, 1997.
- [15] A. Goriely and M. Tabor. Nonlinear Dynamics of Filaments II. Nonlinear Analysis. *Physica D*, 105:45–61, 1997.
- [16] A. Goriely and M. Tabor. Nonlinear Dynamics of Filaments III. Instabilities of Helical Rods. *Proc. R. Soc. Lond. A*, 453:2583–2601, 1997.

- [17] A. Goriely and M. Tabor. Nonlinear Dynamics of Filaments. *Preprint*, 1998.
- [18] A. Goriely and M. Tabor. Nonlinear Dynamics of Filaments IV. Spontaneous Looping of Twisted Elastic Rods. *Proc. R. Soc. Lond. A. (in press)*, 1998.
- [19] A. Goriely and M. Tabor. Spontaneous Helix-Hand Reversal and Tendril Perversion in Climbing Plants. *Phys. Rev. Lett.*, 80:1564–1567, 1998.
- [20] J. Guckenheimer and P. J. Holmes. Nonlinear Oscillations, Dynamical Systems, and Bifurcations of Vector Fields. *Springer-Verlag (New York)*, 1983.
- [21] I. D. Iliev and L. M. Perko. Higher Order Bifurcations of Limit Cycles. *J. Differential Equations*, 154, no.2:339–363, 1999.
- [22] Y. Latushkin, Y. Li, and M. Stanislavova. On the Spectrum of the Linearized 2D Euler Operator. *in preparation, University of Missouri - Columbia*, 2000.
- [23] Y. Li. Bäcklund-Darboux Transformations and Melnikov Analysis for Davey-Stewartson II Equations. *J. Nonlinear Sci.*, 10, No.1:103–131, 2000.
- [24] Y. Li. A Lax Pair for the 2D Euler Equation. *Submitted to Physics Letters A*, 2000.
- [25] Y. Li. On 2D Euler Equations: Part I. On the Energy-Casimir Stabilities and The Spectra for Linearized 2D Euler Equations. *J. Math. Phys.*, 41, No.2:728–758, 2000.
- [26] Y. Li and D. W. McLaughlin. Homoclinic Orbits and Chaos in Perturbed Discrete NLS System. Part I Homoclinic Orbits. *Journal of Nonlinear Sciences*, 7, 1997.
- [27] V. K. Melnikov. On the Stability of the Center for Time Periodic Perturbations. *Trans. Moscow Math. Soc.*, 12:1–57, 1963.
- [28] V. Rom-Kedar. Secondary Homoclinic Bifurcation Theorems. *Chaos*, 5, no.2:385–401, 1995.
- [29] R. Roussarie. On the Number of Limit Cycles Which Appear by Perturbation of Separatrix Loop of Planar Vector Fields. *Bol. Soc. Brasil. Mat.*, 17, no.2:67–101, 1986.
- [30] R. Roussarie. Cyclicité Finie des Lacets et des Points Cuspidaux. *Nonlinearity*, 2, no.1:73–117, 1989.
- [31] J. Sachs. *Text-Book of Botany*. 1975.
- [32] N. Schörghofer, L. Kadanoff, and D. Lohse. How the Viscous Subrange Determines Inertial Range Properties in Turbulence Shell Models. *Physica D*, 88:40–54, 1995.
- [33] S. Wiggins. *Global Bifurcations and Chaos: Analytical Methods*. Springer-Verlag (Berlin), 1988.
- [34] X. Yuan. The Second Order Melnikov Function and Application. *Acta Mathematica Sinica (in Chinese)*, 37(1):135–144, 1994.

- [35] V. E. Zakharov. On the Algebra of Integrals of Motion in Two-Dimensional Hydrodynamics in Clebsch Variables. *Functional Anal. Appl.*, 23, no. 3:189–196, 1989.